ANL-AFCI-177

Argonne NATIONAL LABORATORY

Preliminary Core Design Studies for the Advanced Burner Reactor over a Wide Range of Conversion Ratios

Nuclear Engineering Division

About Argonne National Laboratory

Argonne is a U.S. Department of Energy laboratory managed by UChicago Argonne, LLC under contract DE-AC02-06CH11357. The Laboratory's main facility is outside Chicago, at 9700 South Cass Avenue, Argonne, Illinois 60439. For information about Argonne, see www.anl.gov.

Availability of This Report

This report is available, at no cost, at http://www.osti.gov/bridge. It is also available on paper to the U.S. Department of Energy and its contractors, for a processing fee, from:

U.S. Department of Energy
Office of Scientific and Technical Information
P.O. Box 62
Oak Ridge, TN 37831-0062
phone (865) 576-8401
fax (865) 576-5728
reports@adonis.osti.gov

ANL-AFCI-177

Preliminary Core Design Studies for the Advanced Burner Reactor over a Wide Range of Conversion Ratios

by
E. A. Hoffman, W.S. Yang, and R.N. Hill
Nuclear Engineering Division, Argonne National Laboratory

September 29, 2006

work sponsored by

U. S. Department of Energy,
Office of Nuclear Energy, Science and Technology

UChicago ▶ Argonne LLC

A U.S. Department of Energy laboratory managed by UChicago Argonne, LLC

(This page intentionally left blank)

Table of Contents

List of Tables

List of Figures

Abstract

A consistent set of designs for 1000 MWt commercial-scale sodium-cooled Advance Burner Reactors (ABR) have been developed for both metal and oxide-fueled cores with conversion ratios from breakeven (CR=1.0) to fertile-free (CR=0.0). These designs are expected to satisfy thermal and irradiation damage limits based on the currently available data. The very low conversion ratio designs require fuel that is beyond the current fuel database, which is anticipated to be qualified by and for the Advanced Burned Test Reactor. Safety and kinetic parameters were calculated, but a safety analysis was not performed. Development of these designs was required to achieve the primary goal of this study, which was to generate representative fuel cycle mass flows for system studies of ABRs as part of the Global Nuclear Energy Partnership (GNEP).

There are slight variations with conversion ratio but the basic ABR configuration consists of 144 fuel assemblies and between 9 and 22 primary control assemblies for both the metal and oxide-fueled cores. Preliminary design studies indicated that it is feasible to design the ABR to accommodate a wide range of conversion ratio by employing different assembly designs and including sufficient control assemblies to accommodate the large reactivity swing at low conversion ratios. The assemblies are designed to fit within the same geometry, but the size and number of fuel pins within each assembly are significantly different in order to achieve the target conversion ratio while still satisfying thermal limits.

Current irradiation experience would allow for a conversion ratio of somewhat below 0.75. The fuel qualification for the first ABR should expand this experience to allow for much lower conversion ratios and higher bunrups. The current designs were based on assumptions about the performance of high and very high enrichment fuel, which results in significant uncertainty about the details of the designs. However, the basic fuel cycle performance trends such as conversion ratio and mass flow parameters are less sensitive to these parameters and the current results should provide a good basis for static and dynamic system analysis.

The conversion ratio is fundamentally a ratio of the macroscopic cross section of U-238 capture to that of TRU fission. Since the microscopic cross sections only change moderately with fuel design and isotopic concentration for the fast reactor, a specific conversion ratio requires a specific enrichment. The approximate average charge enrichment (TRU/HM) is 14%, 21%, 33%, 56%, and 100% for conversion ratios of 1.0, 0.75, 0.50, 0.25, and 0.0 for the metal-fueled cores. The approximate average charge enrichment is 17%, 25%, 38%, 60%, and 100% for conversion ratios of 1.0, 0.75, 0.50, 0.25, and 0.0 for the oxide-fueled core. For the split batch cores, the maximum enrichment will be somewhat higher.

For both the metal and oxide-fueled cores, the reactivity feedback coefficients and kinetics parameters seem reasonable. The maximum single control assembly reactivity faults may be too large for the low conversion ratio designs. The average reactivity of the primary control assemblies was increased, which may cause the maximum reactivity of the central control

assembly to be excessive. The values of the reactivity coefficients and kinetics parameters show that some values appear to improve significantly at lower conversion ratios while others appear far less favorable. Detailed safety analysis is required to determine if these designs have adequate safety margins or if appropriate design modifications are required.

Detailed system analysis data has been generated for both metal and oxide-fueled core designs over the entire range of potential burner reactors. Additional data has been calculated for a few alternative fuel cycles. The systems data has been summarized in this report and the detailed data will be provided to the systems analysis team so that static and dynamic system analyses can be performed.

1.0 Introduction

The advanced burner reactor (ABR) will be an integral part of the Global Nuclear Energy Partnership (GNEP). Amongst the goals of GNEP is a more proliferation resistant fuel cycle that operates on a closed fuel cycle. The vision involves Fuel Supplier Nations and User Nations. The User Nations would operate reactors and lease and return their fuel, which most likely would be light water reactors (LWRs) utilizing slightly enriched uranium (UOX) fuel. The Fuel Supplier Nations would operate reactors and the necessary fuel cycle facilities to produce the enriched uranium and close the fuel cycle. In addition to energy production, the ABR would destroy the TRU recovered from the spent UOX fuel in order to close the fuel cycle.

The first ABR will be a prototype or demonstration reactor that will be used to further the project goals of demonstrating the benefits of a closed nuclear fuel cycle and to provide a suitable irradiation facility for development and qualification of transuranic (TRU) fuels for future commercial ABRs. Based on this work, programmatic decisions, cost – benefit analyses, and other unforeseen events, the eventual design of the commercial ABRs is still uncertain and could be based on any of the wide range of designs developed worldwide. There are many options for the ABR from small modular designs to large monolithic designs, which could be pool or loop designs. The fuel will most likely be either U-TRU-Zr alloy metal or oxide. The conversion ratio will be chosen to optimize the cost, performance, and safety of the system. Core design studies are being performed to develop preliminary designs for metal or oxide fuels over a range of conversion ratios. The TRU feed is assumed to result from PWR fuel representative of the near-term operations. The impact of other feed streams will be evaluated.

The ABR design for this study is based on the 1000 MWt SuperPRISM (S-PRISM) reactor. S-PRISM [1] is a pool-type, modular design for a sodium-cooled fast reactor designed to operate as near breakeven or as a breeder. This size is appropriate for a demonstration sized reactor for small modular systems or a prototype of a larger monolithic reactor. Core designs were developed for both metal and oxide fuel, which utilize both internal and radial blankets. The blankets will be removed, even for the breakeven designs. This provides a consistency from high conversion ratio to very low conversion ratio. Then the S-PRISM design will be further modified to produce a range of ABR designs with conversion ratios ranging from breakeven (CR=1.0) to fertile-free (CR=0.0).

The role of the ABR is to transmute the recycled TRU elements which are the dominant contributors to spent fuel radio-toxicity, long-term heat and dose. In order to demonstrate a high TRU consumption rate, it is desirable to have a low conversion ratio. However, a low conversion ratio requires a high TRU enrichment, which is beyond the current irradiation experience with plutonium-based fast reactor fuels. Part of the mission for the first ABR is to irradiate and test high TRU enrichment fuels. It is feasible to design an ABR with variable conversion ratio in a wide range by changing the assembly design only. Conversion ratios greater than approximately 0.65 are within the plutonium enrichments of the U-Pu-10Zr ternary fuel used in the EBR-II and FFTF metal-fuel irradiation test programs [2-4]. This leads to significant uncertainties in the

properties and performance of the low and very low conversion ratio fuels and therefore the appropriate design criteria. However, the current data as it is understood will be utilized along with the necessary assumptions and extrapolations to development preliminary core designs that can quantify the performance over the entire range of conversion ratios and provided detailed systems data for evaluating the static and dynamic GNEP system.

For metal and oxide-fueled cores at CR=1.0, 0.75, 0.50, 0.25, and 0.0, the reactor performance was evaluated in detail including equilibrium cycle core parameters, mass flow, kinetic parameters, and reactivity feedback coefficients. The equilibrium cycle models the equilibrium system where the external cycle for the ABR fuel is modeled and the heavy metal recovered from the ABR fuel is recycled back into the ABR and only TRU and U from external sources is used as needed. The startup performance for each of these designs was evaluated. The startup core is also an equilibrium cycle which models the same core design, but assumes that the ABR fuel is not yet available for self-recycle and all feed material comes from the same external sources as used in the equilibrium calculations. The impact of variations in the external TRU feed from a range of different fuel cycles were analyzed in the CR=0.50 designs.

In Section 2, the computational methods and models used in ABR core design studies are briefly described. The reference S-PRISM design, results using the methods and models used in this study, and a comparison with the General Electrics (GE) results are presented in Section 3. ABR core designs, characteristics, and fuel cycle performance are described in Section 4. This section provides results for equilibrium and startup fuel cycles, thermal characteristics, alternative fuel cycle analysis, systems studies data, reactivity coefficients, and safety parameters. The conclusions are given in Section 5.

2.0 Computational Methods and Models

The ANL suite of fast reactor analysis codes was used to evaluate core performance parameters and reactivity coefficients. Fuel cycle analyses were performed with the DIF3D/REBUS-3 code system [5,6]. Based on the ENDF/B-V.2 data, region-dependent 33-group cross section sets were generated for the metal and oxide-fueled cores with the ETOE-2/MC2-2/SDX code system [7-9]. Using 3-dimensional hexagonal-z geometry models, equilibrium cycle analyses were performed. The model assumes no fuel shuffling and uses batch-average compositions, with the exception of the blankets in the reference S-PRISM designs. The shuffling of the blankets in the S-PRISM was modeled explicitly. Material thermal expansion at operating condition was modeled by adjusting the hexagonal pitch, axial meshes, and the fuel and structure volume fractions appropriately. Irradiation swelling of metal fuel was considered, and the bond sodium was displaced into the lower part of fission gas plenum. Block nuclide depletion was performed by dividing each fuel assembly into five axial depletion zones. For flux calculations, the hexagonal-z nodal diffusion theory option of DIF3D [10] was employed for fuel cycle calculations. The required TRU enrichment (i.e., TRU fraction in heavy metal) was determined from the equilibrium cycle analysis such that the multiplication factor at the end of cycle (EOC) is 1.0 with the rods fully withdrawn from the active core. Enrichment zoning strategy was employed to flatten the power distribution. The fuel cycle length was estimated such that the burnup reactivity swing is within the reactivity control capability of the primary control system. The discharge burnup was determined by adjusting the fuel residence time such that the peak fast fluence is within the fast fluence limit of HT9 cladding (4.0×10^{23} n/cm^2).

Reactivity coefficients and kinetics parameters were calculated for the core configurations at the beginning of equilibrium cycle (BOEC) and the end of equilibrium cycle (EOEC). The coolant, fuel, and structure density coefficients and the coolant void coefficient were determined using the VARI3D perturbation code [11]; the linear perturbation theory option was used for density coefficients, while the exact perturbation theory option was employed for the coolant void coefficient. The effective delayed neutron fraction and prompt neutron lifetime were also calculated using the VARI3D code. The radial and axial expansion coefficients were determined by direct eigenvalue differences of the base and perturbed conditions using the finite-difference option of the DIF3D code.

Detailed isotopic composition of the spent fuel was estimated using the ORIGEN-RA code [12]. The one-group cross sections determined from REBUS-3 equilibrium cycle calculations were used for actinide isotopes, and the LMFBR one-group cross section library of the ORIGEN-RA code package was used for other isotopes.

Linear power limits were estimated by simple thermal-hydraulic calculations based on a single channel model. The coolant inlet and bulk outlet temperatures were 355 °C and 510 °C, respectively. The average flow rate was determined such that the coolant temperature rise across the core is 155 °C. A chopped cosine shape was assumed for the axial power distribution. Hot

channel factors of 2.67, 1.10, 1.48 and 1.24 were used for the film, cladding, gap and coolant regions, respectively.

For U-TRU-Zr ternary metal fuel, the fresh fuel thermal conductivity was determined as a function of U, TRU, and Zr weight fractions using the correlation for U-Pu-Zr fuel [13], and a porosity correction factor of 0.5 was applied to take into account the irradiation effects. It was noted that this metal fuel correlation significantly underestimates the thermal conductivity for high TRU fractions greater than 30%. A minimum thermal conductivity of 10 W/m-K was assumed and with the porosity correction factor of 0.5, the minimum thermal conductivity used in the calculations is 5 W/m-K. The fuel solidus temperature was also estimated as a function of constituent mole fractions using the correlation for U-Pu-Zr fuel [14]. The fuel solidus temperature declines with increasing TRU fraction. As a result, the Zr fraction was assumed to increase at TRU enrichments above 30% TRU/HM. The Zr fraction was 10 w/o below 30% TRU/HM and increased linearly with enrichment to 40 w/o Zr at 100% TRU/HM. The fuel cladding eutectic temperature was conservatively assumed to be limited to 650 °C for all enrichments. Figure 2.1 shows the fuel solidus temperature limit, Zr weight fraction and thermal conductivity at 850 C. The thermal conductivity is a function of temperature with increased thermal conductivity at higher temperatures. The fuel average temperature was used to calculate the thermal conductivity used in the estimation of the linear power limit.

For mixed oxide fuel, the thermal conductivity and melting temperature correlations of Reference 15 were used, and the porosity correction factor of 0.75 was applied for thermal conductivity. Figure 2.2 shows the fuel solidus temperature limit and thermal conductivity at 1300 C. There is no data available for the thermal conductivity of oxide fuel with the PuO2 concentration over 30%, but the correlation was assumed to be valid. The dominant factor for thermal conductivity correlation used for the oxide fuel is temperature and the thermal conductivity increases with temperatures. The fuel average temperature was used to calculate the thermal conductivity used in the estimation of the linear power limit.

The linear power limit was determined such that the peak fuel centerline temperature is lower than the fuel solidus temperature. For metal fuel, linear power was additionally limited such that the peak cladding inner-wall temperature is lower than the fuel cladding eutectic temperature.

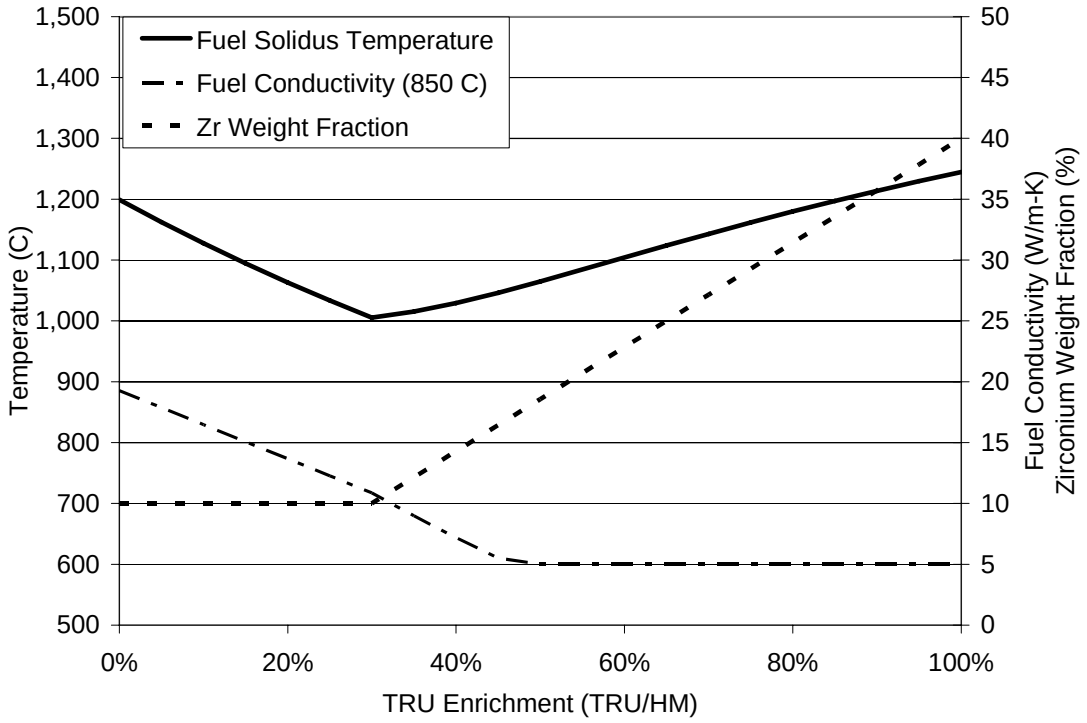

Figure 2.1 Assumed Properties of U-TRU-Zr Metal Fuel.

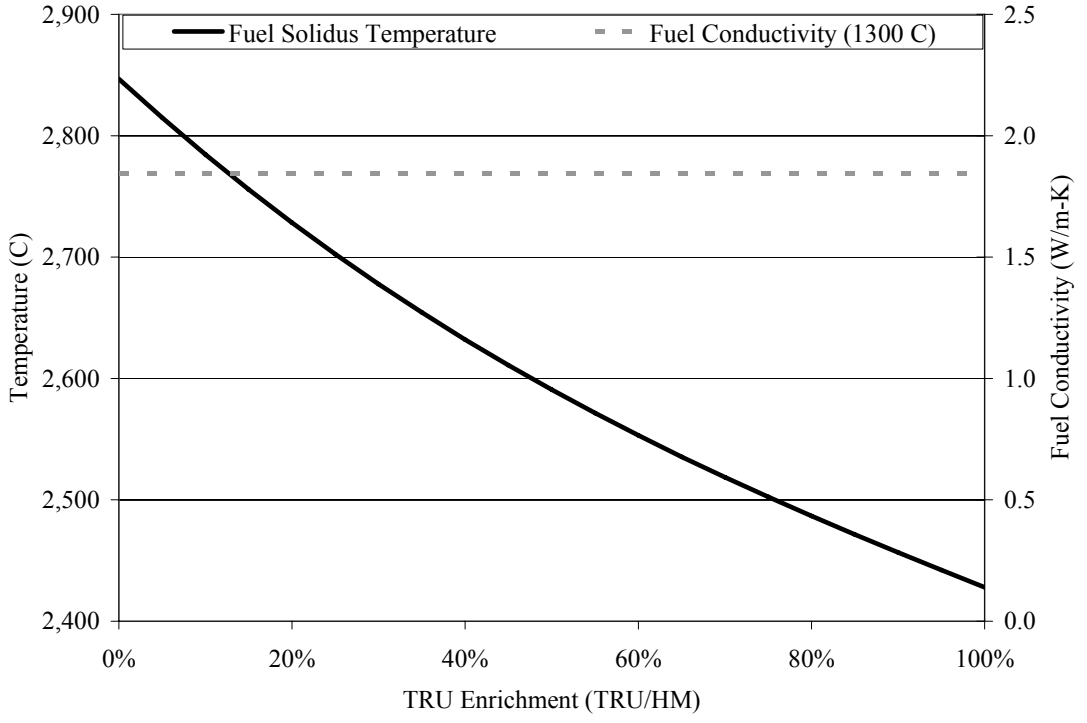

Figure 2.2 Assumed Properties of (U,TRU)O_2 Fuel.

The goal of this study was to develop potential ABR core designs over a wide range of conversion ratios. To allow for a transition to higher or lower conversion ratios as required, it would be desirable to retain as similar design as possible in order. The overall assembly dimensions were retained, while the number and size of fuel pins within each assembly are adjusted to achieve the target conversion ratio, while still satisfying the imposed design criteria. The fuel volume fraction is adjusted by varying the fuel pin diameter and the linear power is adjusted by varying the number of fuel pins per assembly. Most other parameters are assumed fixed (e.g., assembly dimensions, active height).

By reducing the pin diameter the fuel volume fraction is reduced, which requires a higher TRU enrichment for the same fuel cycle. The higher TRU enrichment increases TRU fission relative to U-238 capture, which reduces the TRU conversion rate. This is the fundamental method used to vary the conversion ratio.

From a manufacturing standpoint, it is desirable to minimize the number of fuel pins that must be produced. However, the thermal performance of the fuel degrades as the TRU enrichment increases, which at some point necessitates reducing the average linear power. This was achieved by increasing the number of fuel pins per assembly. This requires the fuel pin diameter to be reduced even further to maintain the necessary fuel volume fraction for the target conversion ratio.

The reference pins are wire wrapped pins. The reduction in conversion ratio necessitates a reduction in fuel volume fraction, which results in an increased pitch to diameter ratio, which would require a larger wire wrap diameter. At very low conversion ratios, the wire wrap diameter becomes very large relative to the fuel pin. This suggests a benefit in utilizing spacer grids at the very low conversion ratios. It was assumed that the wire wrap volume would not exceed 2.5% of the assembly volume, which seems close to the volume fraction of grid spacers in designs that have utilized them. When this value was exceeded, it was assumed that grid spacers would be utilized and would occupy 2.5% of the assembly volume. Also, a number of structural pins must replace the fuel pins to provide support for the grids while allowing the fuel pins to grow within the grid structure. For all designs, seven structural pins were assumed. The structural pins are simply steel tubes and were assumed to have the same outer diameter as the fuel pins, but are 20% thicker than the cladding.

No fuel shuffling is utilized. Three enrichment zones were utilized to produce a more uniform radial power distribution. Except for the CR~0.0 cases, an enrichment splitting of 1.0, 1.25, and 1.50 was assumed. This means that the enrichment of the middle core is 1.25 times the inner core and the outer core is 1.50 times the enrichment of the inner core. The number of assemblies in the inner, middle, and outer core varies with conversion ratio. Although, no attempt was made to optimize the enrichment splitting further, there was not a significant shift in power from beginning to end of cycle as shown by the power peaking factors remaining relatively unchanged.

The fuel residence time is limited by the cladding fluence, which means that without fuel shuffling the outer fuel assemblies can remain in the core longer than the inner fuel assemblies. To maximize the average discharge burnup, the fuel assemblies near the periphery general remained in the core an additional cycle or two so that the cladding fluence would be near the limit.

In general it is desirable to maximize the cycle length in order to minimize the fraction of time shutdown for refueling. However, the low conversion ratio designs have very large burnup reactivity swing rates. This requires a large excess reactivity at the beginning of cycle, which presents a large potential reactivity insertion from an assembly withdrawal accident. Managing this large burnup reactivity swing is a tradeoff between a reduced capacity factor due to more frequent refueling and a larger core size due to more control assemblies. There is no hard limit on the reactivity limit of a single control assembly, and there are options such as such as rod stops or mechanical limits on withdrawal rates. For example, the PRISM design introduced a rod stop system to limit the maximum withdrawal worth to \$0.3, and the FFTF used a control circuit that limits the rod withdrawal speed to 9.8 inch/min. However, it would likely be simpler to design the control system if the amount of reactivity per assembly is limited to at least below \$1 and ideally to an even smaller value with \$0.30 per assembly assumed to be a target value [16]. At each lower conversion ratio, a judgment was made on whether to increase the number of control assemblies, reduce the cycle length, and/or allow the reactivity of the average primary control assembly to increase. Detailed safety analysis will be required to determine if these low conversion ratio designs have adequate safety margins. Previous studies of low conversion ratio metal-fueled cores [17] suggest that the metal-fueled cores will have satisfactory safety characteristics. Cost estimates will need to be performed to evaluate the tradeoff between more control assemblies and shorter cycle lengths.

3.0 S-PRISM Reference Designs

The primary goal was to assess the performance of a commercial-scale fast burner reactor. The PRISM design has been developed over many years with joint efforts of the Department of Energy, and General Electrics and has been reviewed and analyzed by many other organizations. The S-PRISM was a GE extension of the PRISM reactor after the joint effort with DoE that is supposed to be more economical than previous versions because of increased size and design simplifications. Therefore, this seemed to be the logical choice for the reference design of this study.

The S-PRISM is a modular plant which is based on 1000 MWt reactor cores. The core has design options for metal and oxide fuel and utilizes internal and external blankets to produce a TRU breakeven design with a conversion ratio slightly above 1.0. Additional options include axial blankets to increase the conversion ratio substantially above 1.0 for production of surplus TRU for startup of additional fast reactors. One of the objectives of the GNEP program is to minimize proliferation concerns, which would suggest a desire to eliminate the high quality plutonium stream that result from blankets. Additionally, the ABR is envisioned as a burner reactor that would consume the TRU produced in LWR deployed in User Nations. Therefore, even high conversion ratios designs were designed without blankets in this study. The S-PRISM driver fuel without blankets would have a conversion ratio of approximately 0.8.

The S-PRISM design input, layout, and results for metal and oxide-fueled core designs for near TRU breakeven (no axial blankets) are provided in Ref. 1. Figure 3.1 and Figure 3.2 show the reactor layout for the metal and oxide-fueled S-PRISM designs, respectively.

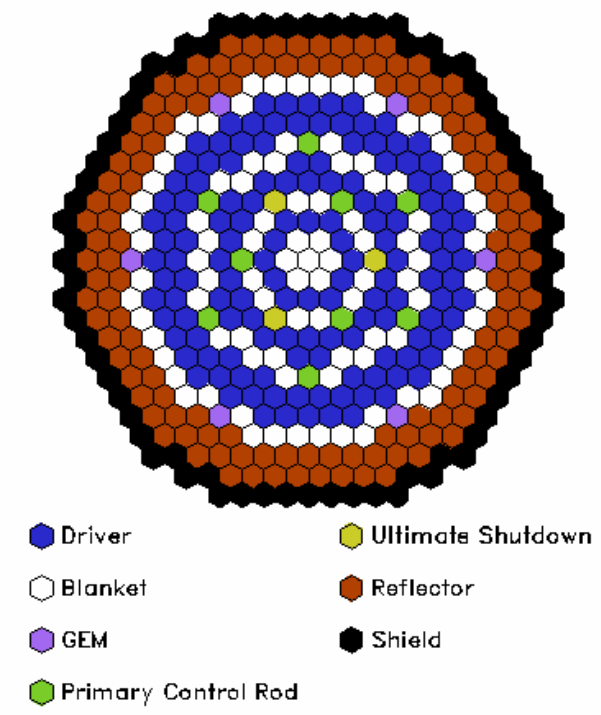

Figure 3.1 Reference S-PRISM Metal-Fueled Core Layout

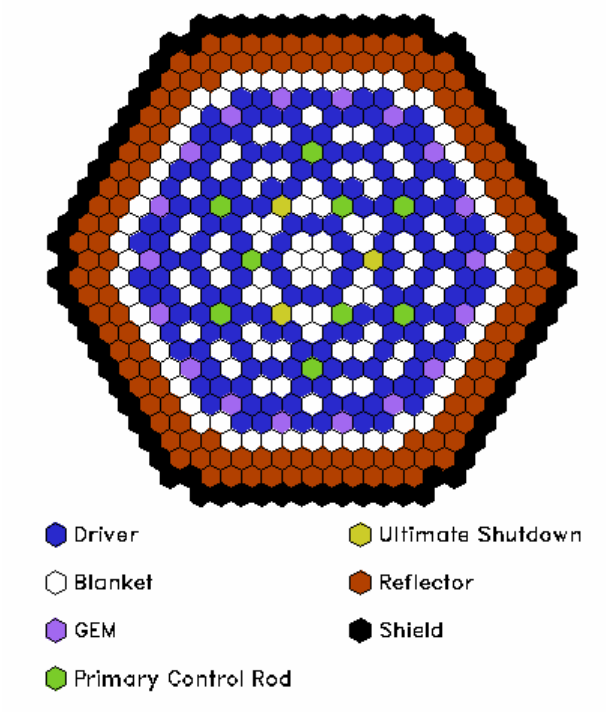

Figure 3.2 Reference S-PRISM Oxide-Fueled Core Layout

The performance of the metal and oxide-fueled S-PRISM designs was calculated using the same methodology that will be utilized in the evaluation of the ABR. Table 3.1 summarizes the results. There were some uncertainties in the design outside of the core region. The shuffle pattern was provided for all blanket assemblies, except the treatment of the central blanket assemblies was not provided. These differences prevent an exact comparison with the GE results. The mass flow parameters and core loading were generally in very good agreement. The peak burnup in the driver was overestimated in the oxide core. GE uses a limit of 180 MWd/kg, which would not be satisfied according to this analysis. The irradiation damage was limited solely by fast neutron fluence limits in this analysis because of uncertainties in the actual limits in high TRU concentration fuels and for a consistent comparison. Fuels beyond this burnup will need to be qualified as part of the mission of the first ABR. The peak fast fluence showed very good agreement. This analysis calculated a higher peak linear power for the metal-fueled design.

The burnup reactivity loss is small for the metal-fueled cores with GE predicting a small reactivity loss and this analysis predicting a small reactivity gain. The depletion was performed with control assemblies withdrawn from the core, while the GE analysis most likely assumed partial insertion of the control assemblies for the depletion calculation, which is consistent with the difference in burnup reactivity loss for the metal-fueled case. However, the burnup reactivity loss are not in agreement for the oxide case with GE reporting a nearly 1% Δk and a calculated value of essentially zero. The difference is in the direction that would be expected for depletion with and without the control assemblies partially inserted in the core, but the magnitude of the difference is much large than was expected. The reason for this large difference was not

determined, but since most other parameters showed good agreement, it was not pursued further, but must be resolved as the design development progresses. If the burnup reactivity loss is significantly underestimated, additional control assemblies and or shorter cycle lengths may be required, but the transmutation performance, mass flows, and fuel assembly design will not change significantly.

Table 3.1 Performance Comparison of S-PRISM Core Designs

		Metal		Oxide	
		GE	ANL	GE	ANL
BOC Heavy Metal Loading (kg)		26,092	26,181	34,926	34,914
BOC TRU Loading		3,078	3,191	5,208	5,416
BOC Fissile Pu		2,336	2,309	3,469	3,488
BOC U Loading		23,014	22,989	29,719	29,499
EOC TRU Loading		3,133	3,247	5,282	5,479
TRU Consumption Rate (kg/yr)		-33.6	-34.3	-38.6	-37.3
Burnup, MWd/kg	Average Driver	106.0	105.7	116.0	116.5
	Peak Driver	149.0	144.1	178.0	194.7
Peak Fast Fluence, 10^{23} n/cm^2	Driver	3.71	3.87	2.96	3.04
	Blanket	3.90	4.01	2.44	2.40
Burnup Reactivity Loss (Δk)		0.12%	-0.10%	0.98%	-0.02%
Average Linear Power (kW/m)		18.9	19.1	16.0	16.2
Peak Linear Power (kW/m)	Driver	30.4	34.9	30.1	29.5
	Blanket	40.3	41.9	27.2	27.8
Peak Neutron Flux (10^{15} n/cm2-s)	Total	3.62	3.80	2.38	2.42
	Fast	2.47	2.58	1.38	1.42

4.0 Reference ABR Core Designs, Characteristics, and Fuel Cycle Performance

Reference ABR core designs have been developed for metal and oxide-fueled options. The reference ABR designs are compact cores that have been designed to satisfy a number of design criteria while trying to maximizing the average linear power and fuel discharge burnup. The reference designs were developed for an equilibrium fuel cycle with the fast reactor fuel recycled and an external supply of TRU used for makeup. The makeup TRU for the reference design was recovered from the spent nuclear fuel (SNF) from advanced light water reactors (LWR) that was irradiated to 50 GWd/MT and stored for five years prior to reprocessing. The makeup uranium was assumed to be depleted uranium. The reference designs were developed for target conversion ratios of 1.0, 0.75, 0.50, 0.25, and 0.0 for both metal and oxide fuel. Some additional analysis was performed to evaluate startup performance and the effect of different TRU feed streams, but all aspects of the reference design remained unchanged except for the composition of the external feed and whether or not the fast reactor fuel was recycled.

4.1. Design Development Summary

The primary goal was to develop 1,000 MWt ABR core designs that ranged from TRU breakeven (CR~1.0) to fertile-free (CR~0.0) to determine the representative fuel cycle performance characteristics to be used in systems studies. A number of design criteria were imposed on the design to avoid major design modifications as more detailed design analysis is performed and therefore provide fuel cycle characteristics for the systems studies that are as representative as possible for this level of analysis. The available fuel database is insufficient, which results in uncertainty and the designs may exceeded design limits or could be far from optimum.

One criterion that is important to optimizing the design for the very low conversion ratio designs is the minimum practical fuel pin diameter. The pins were made as small as necessary to achieve the target conversion ratio and satisfy the linear power limits based on the assumed properties at high enrichments. Because of uncertainties in the fuel properties at high TRU content, the number of fuel pins per assembly may be excessive. If the properties prove better than used in this analysis, the linear power limit will increase and a smaller number of pins per assembly, each with a larger diameter than assumed in this analysis, would be utilized. However, the fuel volume fraction, mass flow, and other parameters would likely remain relatively unchanged. If these designs with the large number of very small diameter pins are required to satisfy thermal limits, but ultimately prove impractical, it will be necessary to increase the pin diameter while still satisfying the other criteria. This would require a reduced power density and an increase in the core size. This would have a significant impact on the mass flow and other performance characteristics.

The first step in developing the designs was to convert the S-PRISM layout into a breakeven design without blankets. Three TRU enrichment zones were utilized to produce a more uniform power distribution, but all assembly and fuel pin designs are otherwise identical. This is referred

to as the blanket-free case throughout. It eliminates the highest quality plutonium stream that would result from irradiating blankets. The exact S-PRISM layout was used and all driver and blanket assemblies were replaced with a single fuel assembly type that is intermediate in design to the original driver and blanket assemblies. The minimum number of pins that still satisfy the linear power limits and the diameter of these pins that would result in a conversion ratio of approximately 1.0 was determined.

It would be possible to reduce the fuel pin diameter and retain this layout at much lower conversion ratio. However, it is generally desirable to reduce the core diameter to improve economics and this was assumed to be the case. There would be large thermal margins if the S-PRISM driver assemblies would be used in these large cores. By reducing the number of fuel assemblies to close to the same number as the driver assemblies in the S-PRISM design, the fuel would be expected to be near the thermal limits because the driver assemblies carry most of the power. This results in a core configuration of 8 rings of fuel and control assemblies. The Gas Expansion Modules (GEM) assemblies were not used in these designs, but could be added at the core periphery if deemed necessary. This would result in little impact on the design or performance, except for reactivity coefficients. Future safety analysis is needed to evaluate the safety performance of any of these configurations.

The breakeven core has a very low reactivity swing and therefore does not require a large number of control assemblies and can operate with longer cycle lengths. The 9 primary control assemblies used in the S-PRISM should be more than adequate. Because of the higher power density, the core residence time of the fuel was reduced substantially. A minimum of three cycles for the inner core was assumed and the cycle length was adjusted to just satisfy the fluence limit.

The CR~0.75 design has a much larger burnup reactivity swing rate than the breakeven design. Therefore, it was decided to replace seven fuel assemblies with seven primary control assemblies. This maintained the reactivity per control assembly near the $0.30 goal without dramatically reducing the cycle length.

The CR~0.5 design could easily benefit from more control assemblies. However, it was decided to maintain the 16 primary control assemblies, not reduce the cycle length significantly, and allow the reactivity swing per control assembly to increase. The value is much higher, but still well below $1 per control assembly.

The CR~0.25 has slightly different designs between the metal and oxide. Even after reducing the cycle length to less than one half year, an additional six primary control assemblies were needed for the metal-fueled core. They were not predicted to be needed for the oxide core.

The CR~0.0 design has 22 primary control assemblies and cycle lengths less than a half-year. In order for the conversion ratio to be near zero, the fuel must be essentially uranium free. The actual conversion ratio will be slightly above zero at equilibrium for a uranium free makeup stream. Assuming all the in situ produced uranium, mostly U-234, will be recycled, the calculated conversion ratio will be slightly above zero and the TRU enrichment will be slightly

less than 100%. This precludes using enrichment splitting to flatten the radial power distribution. Slightly large fuel pins were used for the middle and outer core assemblies to increase the reactivity of these regions which serves the same function as increased enrichment.

Generally, the designs have maximized the fuel residence time based on the fast fluence limit. However, many designs exceed the current fuel database for enrichment and/or burnup. The very low enrichment designs require high enrichments and very low fuel volume fractions. This results in a very large number of very small diameter pins that may present practical challenges to their production. Further optimization and development of the designs is expected as better understanding of the low conversion ratio fuel performance is gained from on-going fuel development. The current results using consistent assumptions and methods should provide a good estimate of the relative performance of future commercial-scale ABRs over the entire range of conversion ratios. The following sections will summarize the results of this analysis and compare the expected performance of the ABR from breakeven to uranium-free designs.

4.2. Design Summary

The S-PRISM core layouts were provided in Figure 3.1 and Figure 3.2. Section 4.1 discussed the evolution from the S-PRISM layout to the compact fertile-free layout. This section discusses the overall core configuration (Section 4.2.1) and fuel assembly designs (Section 4.2.2) for the different designs that were developed.

4.2.1. Core Configuration

Core configurations were developed for metal and oxide-fuel options with conversion ratios from breakeven (CR=1.0) to fertile-free (CR=0.0). Figure 4.1 and Figure 4.2 show the layout of the breakeven core using the S-PRISM layout and a blanket-free design with variable TRU enrichment. Figure 4.3 and Figure 4.4 show the layouts of the metal and oxide-fueled cores of different conversion ratios. Table 4.1 and Table 4.2 summarize the configurations of the metal and oxide-fueled ABRs respectively.

The number of driver plus blanket assemblies was reduced from 235 for the metal fuel and 295 for the oxide fuel to between 151-144. As a result, the diameter of the reactor can be reduced by approximately 0.6 m for the metal-fueled core and 0.9 m for the oxide-fueled core. This would be expected to result in significant cost savings for the reactor vessel and all components whose size is impacted by the core diameter.

As the conversion ratio is reduced the burnup reactivity swing will likely require an increased number of primary control assemblies to safely compensate. As can be seen, the breakeven configuration retains the same number of control assemblies as the S-PRISM design and the zero conversion ratio design has an additional 13 primary control assemblies. The need for additional secondary control assemblies was not evaluated. There was also a shift of more inner core assemblies and less middle and outer core assemblies at lower conversion ratios. The lower fuel volume fraction increases neutron leakage, which seems to flatten the radial power

distribution. All of these cores are approximately the same size and could be adapted to fit use the same vessel and grid plate, but some flow modification would be required. This would allow a given reactor to operate at much higher conversion ratios if designed with adequate control and shutdown assemblies for lower conversion ratios.

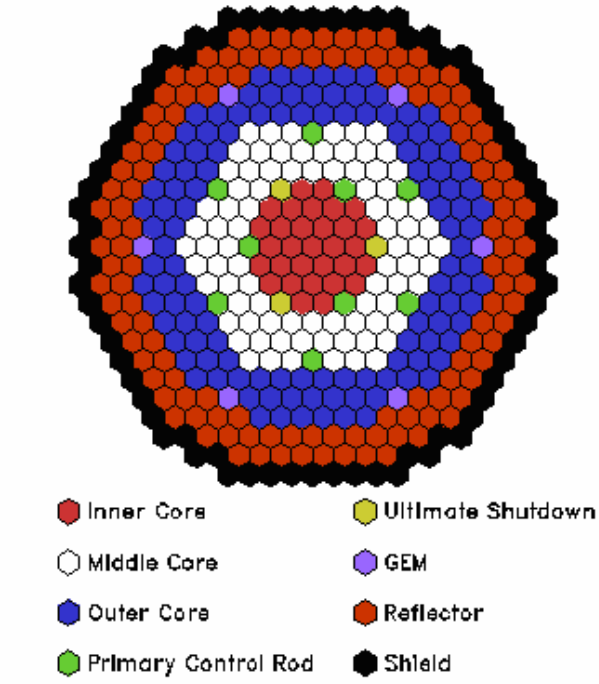

Figure 4.1 Breakeven Metal-Fueled ABR Core Layout Using S-PRISM Layout

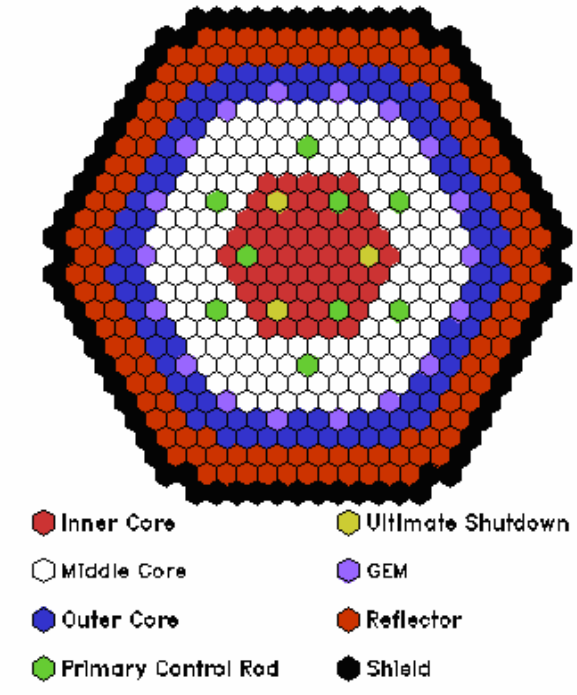

Figure 4.2 Breakeven Oxide-Fueled ABR Core Layout Using S-PRISM Layout

Table 4.1 Core Design of Metal-Fueled ABR

	S-PRISM Layout		Compact Core				
	S-PRISM	Blanket-free	1.0	0.75	0.50	0.25	0.00
Driver	138	235	151	144	144	144	144
- Inner (Lowest Enrichment)		*31*	*19*	*30*	*42*	*48*	*78*
- Middle (Medium Enrichment)		*84*	*66*	*42*	*66*	*54*	*24*
- Outer (Highest Enrichment)		*120*	*66*	*72*	*36*	*42*	*42*
Blanket	97	0	0	0	0	0	0
Primary Control Assemblies	9	9	9	16	16	22	22
Secondary Control Assemblies	3	3	3	3	3	3	3
Gas Expansion Modules	6	6	0	0	0	0	0
Reflector	126	126	90	90	90	84	84
Shield	72	72	60	60	60	60	60
Equivalent core diameter, m	2.71	2.71	2.18	2.18	2.18	2.22	2.22
Equivalent reactor diameter, m	3.62	3.62	3.02	3.02	3.02	3.02	3.02

Table 4.2 Core Design of Oxide-Fueled ABR

	S-PRISM Layout		Compact Core				
	S-PRISM	Blanket-free	1.0	0.75	0.50	0.25	0.00
Driver	162	295	151	144	144	144	144
- Inner (Lowest Enrichment)	*162*	*55*	*19*	*72*	*72*	*72*	*78*
- Middle (Medium Enrichment)		*144*	*66*	*36*	*36*	*36*	*24*
- Outer (Highest Enrichment)		*96*	*66*	*36*	*36*	*36*	*42*
Blanket	133	0	0	0	0	0	0
Primary Control Assemblies	9	9	9	16	16	16	22
Secondary Control Assemblies	3	3	3	3	3	3	3
Gas Expansion Modules	18	18	0	0	0	0	0
Reflector	138	138	138	102	102	102	84
Shield	78	78	60	60	60	60	60
Equivalent core diameter, m	3.07	3.07	2.18	2.18	2.18	2.18	2.22
Equivalent reactor diameter, m	3.97	3.97	3.24	3.07	3.07	3.07	3.02

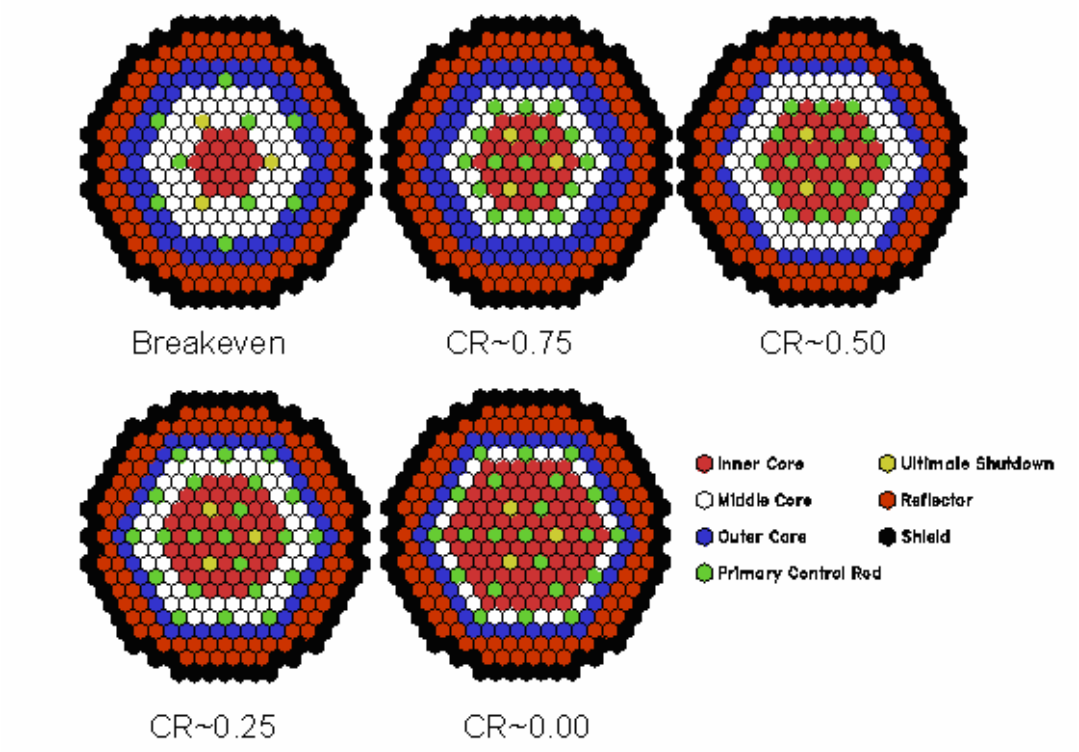

Figure 4.3 Metal-Fueled ABR Core Layouts for a Range of Conversion Ratios

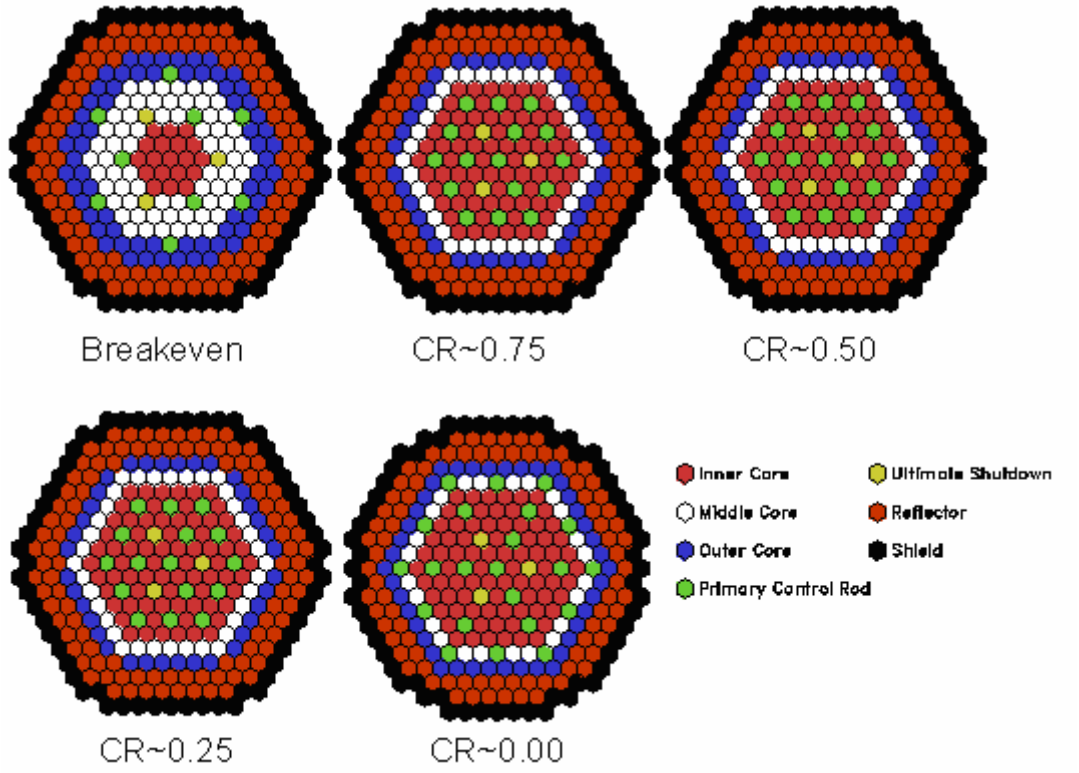

Figure 4.4 Oxide-Fueled ABR Core Layouts for a Range of Conversion Ratios

4.2.2. Assembly Designs

The dimensions of fuel ducts for all the fuel assemblies for the metal and oxide-fueled core designs are the same, which would increase the likelihood of interchangeable designs. Table 4.3 provides the overall dimensions of the fuel assemblies. However, the oxide-fueled core was 36 cm taller than the metal-fueled core in the S-PRISM designs and this difference was retained for the ABR. Optimization of the design would determine if the height should be increased or decreased. A simple model was used to estimate if sufficient plenum height was available for fission gas release. The results suggest that for most designs it is sufficient with a few exceptions where small increases may be required, but the results suggest only minor changes and were neglected, but would need to be verified with detail analysis to ensure cladding integrity. The non-fuel assembly designs were based on the Advanced Burner Test Reactor (ABTR) design study. However, it was decided to bypass a small test reactor and proceed to a larger demonstration or prototype reactor. Despite a larger assembly pitch, the material volume fractions were assumed to be the same as used in the ABTR design [18]. The details of the room temperature fuel pin designs and volume fractions are provided in Table 4.4 and Table 4.5 for the metal and oxide-fueled assembly designs, respectively.

Table 4.3 Assembly Dimensions

	Metal or Oxide
Assembly pitch, cm	16.142
Inter-assembly gap, cm	0.432
Duct outside flat-to flat distance, cm	15.710
Duct material	HT9
Duct thickness, cm	0.394

The CR=0.0 designs require the smallest diameter fuel pins because of the need for the lowest fuel volume fraction and the lowest linear power. This results in a very large number of very small pins in the reactor. There certainly are cost and possibly technical challenges associated with producing these pins. Typical commercial driver pins have diameters similar to the designs with conversion ratios in the 0.5 to 0.75 range. However, experimental reactors have used fuel pins with outer diameters as small as 0.4 cm in the FERMI reactor [19], which is as small as the smallest diameter pins in this study. This will need to be evaluated in more detail if very low conversion ratio designs are deemed desirable.

If a very low conversion ratio is desired, it is likely that it would be more practical to reduce the assembly size and spread the pins amongst a greater number of assemblies that would occupy approximately the same core diameter. This would be particularly beneficial for fuel management because of the small fraction (less than 10%) of the fuel assemblies replaced during each refueling and the need to increase the number of primary control assemblies.

The CR=0.0 designs used three different pin diameters to flatten the radial power distribution. Since the enrichment is 100% for CR=0.0, the variable pin diameter allows variable fuel volume fraction that allow for flattening of the radial power distribution by loading the

higher fuel volume fraction (larger pin diameter) assemblies near the core periphery. The CR=0.0 metal-fueled design shows spacer grids for two of the three assembly types and wire wrap for the third. Spacer grids would probably be used for all, but this anomaly was not noted until after all the calculations were completed and the data provided is how it was modeled. This will have negligible impact on any of the results.

Figure 4.5 shows the volume fraction of each fuel assembly. The values for the zero conversion cases are the assembly weighted core average. There is some variation in all the volume fractions, but effectively fuel is being replaced by coolant as the conversion ratio is reduced. The fuel volume fraction has to increase from the larger core layout of the S-PRISM to the compact core configuration to compensate for the increased neutron leakage of the smaller core. The slightly higher fuel volume fraction of the CR=0.0 metal-fueled core relative to the CR=0.25 metal-fueled core is a result of the increased zirconium fraction in the metal fuel and the utilization of different diameter pins.

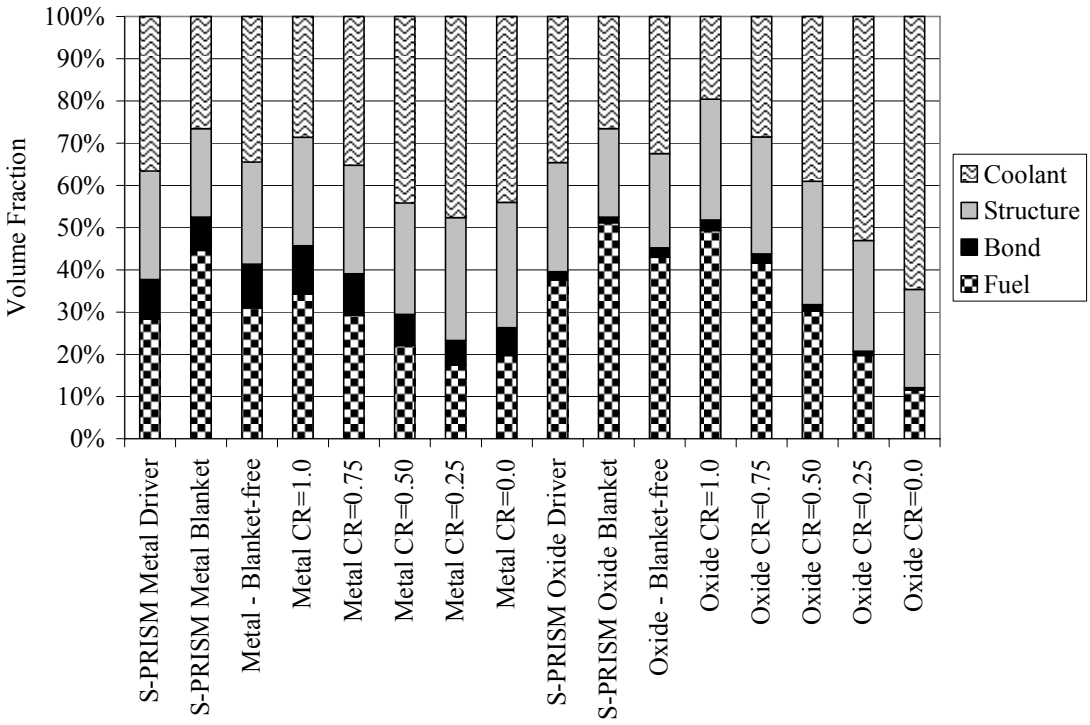

Figure 4.5 Fuel Assembly Volume Fractions.

Table 4.4 Metal-Fueled Assembly Designs

	S-PRISM		Blanket-free	Compact Core						
	Driver	Blanket	1.0	1.0	0.75	0.50	0.25	0.00		
								Inner	Middle	Outer
Fuel pins per assembly	271	127	217	271	271	324	540	540	540	547
Spacer type	Wire	Wire	Wire	Wire	Wire	Grid	Grid	Grid	Grid	Wire
Structural pins per assembly	0	0	0	0	0	7	7	7	7	0
Pin data										
- Bond material	Na	Na	Na	Na	Na	Na	Na	Na	Na	Na
- Height (core), cm	101.60	101.60	101.60	101.60	101.60	101.60	101.60	101.60	101.60	101.60
- Height (plenum), cm	191.14	191.14	191.14	191.14	191.14	191.14	191.14	191.14	191.14	191.14
- Overall pin length, cm	407.04	407.04	407.04	407.04	407.04	407.04	407.04	407.04	407.04	407.04
- Fuel smeared density, % TD	75	85	75	75	75	75	75	75	75	75
- Fabrication density, % TD	100	100	100	100	100	100	100	100	100	100
- Pin diameter, cm	0.744	1.201	0.852	0.808	0.755	0.623	0.464	0.449	0.494	0.539
- Pin pitch-to-diameter ratio	1.191	1.078	1.163	1.100	1.176	1.293	1.357	1.400	1.273	1.167
- Cladding thickness, cm	0.0559	0.0559	0.0559	0.0559	0.0559	0.0559	0.0559	0.0559	0.0559	0.0559
- Wire wrap diameter, cm	0.1422	0.0940	0.1385	0.0805	0.1329	N/A	N/A	N/A	N/A	0.0900
Volume fraction, %										
- Fuel	28.30	44.61	31.02	34.26	29.30	22.08	17.44	16.04	20.60	26.05
- Bond	9.43	7.87	10.34	11.42	9.77	7.36	5.81	5.35	6.87	8.68
- Structure	25.70	20.97	24.16	25.73	25.68	26.41	29.15	28.53	30.45	31.36
- Coolant	36.57	26.54	34.48	28.59	35.25	44.15	47.60	50.08	42.09	33.90

Table 4.5 Oxide-Fueled Assembly Designs

	S-PRISM		Blanket-free	Compact Core						
	Driver	Blanket	1.0	1.0	0.75	0.50	0.25	0.00		
								Inner	Middle	Outer
Fuel pins per assembly	217	127	127	271	271	324	324	324	324	324
Spacer type	Wire	Wire	Wire	Wire	Wire	Grid	Grid	Grid	Grid	Grid
Structural pins per assembly	0	0	0	0	0	7	7	7	7	7
Pin data										
- Bond material	He	He	He	He	He	He	He	He	He	He
- Height (core), cm	137.16	137.16	137.16	137.16	137.16	137.16	137.16	137.16	137.16	137.16
- Height (plenum), cm	170.82	191.14	170.82	170.82	170.82	170.82	170.82	170.82	170.82	170.82
- Overall pin length, cm	422.28	407.04	422.28	422.28	422.28	422.28	422.28	422.28	422.28	422.28
- Fuel smeared density, % TD	85	93	85	85	85	85	85	85	85	85
- Fabrication density, % TD	89.4	95.4	89.4	89.4	89.4	89.4	89.4	89.4	89.4	89.4
- Pin diameter, cm	0.894	0.954	1.138	0.868	0.808	0.658	0.556	0.438	0.460	0.482
- Pin pitch-to-diameter ratio	0.991	1.295	1.130	1.023	1.099	1.224	1.448	1.839	1.751	1.672
- Cladding thickness, cm	1.1642	1.0782	0.0635	0.0635	0.0635	0.0635	0.0635	0.0635	0.0635	0.0635
- Wire wrap diameter, cm	0.1727	0.1294	0.1476	0.0198	0.0797	N/A	N/A	N/A	N/A	N/A
Volume fraction, %										
- Fuel	37.63	51.17	42.99	49.29	41.65	30.22	19.73	10.36	11.87	13.49
- Bond	1.95	1.32	2.23	2.55	2.16	1.56	1.02	0.54	0.61	0.70
- Structure	25.85	20.97	22.31	28.58	27.71	29.22	26.22	22.75	23.40	24.04
- Coolant	34.57	26.54	32.48	19.58	28.48	39.00	53.02	66.35	64.11	61.77

4.3. Equilibrium Performance Characteristics

The core performance characteristics of the reference cores are discussed in this section. These were obtained from REBUS-3 equilibrium cycle calculations with recycling. The equilibrium cycle models the equilibrium system where the external cycle for the ABR fuel is modeled and the heavy metal recovered from the ABR fuel is recycled back into the ABR and only TRU and U from external sources is used as needed.

A significant factor in the overall performance of the reactor would be capacity factor. The capacity factor will be dependent on the conversion ratio because of differences in refueling frequency, number of assemblies replaced per outage, and unplanned outages related to fuel failures. An 85% capacity factor was assumed in the models used to evaluate the performance, but all results are reported in effective full power days (EFPD) or years (EFPY). These results can then be multiplied by the appropriate capacity factor when it is determined.

4.3.1. Thermal Performance

As aforementioned, the fuel volume fraction was adjusted to achieve the target conversion ratio, while the number of individual fuel pins per assembly was adjusted to satisfy linear power limits. The thermal characteristics of each design are provided in Table 4.6 and

Table 4.7 for the metal and oxide-fueled cores, respectively. As a result of lower thermal conductivity and/or solidus temperature, the linear power limit decreases with increasing enrichment (lower conversion ratio).

The metal-fueled CR=0.0 core is calculated to have a larger margin because the larger diameter fuel pins in the outer ring of the core, increase the fuel mass and reduce the maximum swing in power level from charge to discharge. This is important because the assemblies are assumed to have a fixed orifice, which is set to have a specific core average temperature rise. Variation in assembly power over their lifetime requires individual assembly to have a greater temperature rise than the core average for some of their lifetime and the greater the swing the higher the peak outlet temperature would be when the assembly is running at its hottest. Higher coolant temperatures reduce the maximum linear power, which is what is causing the lower margin for CR=0.25 relative to the CR=0.0 for the metal-fueled designs. A simple model was used to estimate these values and optimization of the core design and orificing would most likely reduce the differences between designs.

The S-PRISM design had a minimum of 13% power margin to melting. Nearly all designs have significantly larger margins for fuel centerline melting or fuel/cladding eutectic melting. Similar design margins exist between the metal and oxide-fueled cores, but the average linear power is significantly higher for the metal fuel at high conversion ratios and significantly lower at very low conversion ratios because of thermal conductivity variations referred to earlier in Figure 2.1. There is significant uncertainty in the properties of the high and especially very high

enrichment fuels, which may allow for higher average linear powers in the metal fuel at low conversion ratios.

The lower fuel volume fraction leads to a very large increase in specific power for the very low conversion ratio designs. For the CR=0.0 designs, the specific power is over four times that of the breakeven designs.

Table 4.6 Thermal Characteristics of Metal-Fueled Cores

		S-PRISM	Blanket-free	Compact Core				
Conversion Ratio		N/A	1.00	1.00	0.75	0.50	0.25	0.00
Average Linear Power (kW/m)		18.9	18.0	22.4	23.5	19.6	11.7	11.7
Specific power (kW/kg)		N/A	42.5	59.7	74.4	105.8	168.9	276.0
Power peaking factor	BOEC	1.41	1.542	1.649	1.525	1.452	1.528	1.574
	EOEC		1.582	1.720	1.484	1.431	1.508	1.598
Peak Linear Power (kW/m)	Driver	30.42	28.6	38.9	39.3	32.7	21.4	21.0
	Internal Blanket	40.25	N/A	N/A	N/A	N/A	N/A	N/A
	Radial Blanket	30.70	N/A	N/A	N/A	N/A	N/A	N/A
Minimum Power to Centerline Melt		138%	243%	222%	159%	128%	133%	178%
Minimum Power to Surface Eutectic Melt		113%	139%	131%	127%	123%	121%	130%
Average coolant flow rate (kg/s-pin)		N/A	0.11	0.14	0.15	0.12	0.07	0.07

Table 4.7 Thermal Characteristics of Oxide-Fueled Cores

		S-PRISM	Blanket-free	Compact Core				
Conversion Ratio		N/A	1.00	1.00	0.75	0.50	0.25	0.00
Average Linear Power (kW/m)		16.0	19.1	17.5	18.3	15.3	15.2	15.2
Specific power (kW/kg)		N/A	30.4	51.9	65.6	91.7	145.7	255.6
Power peaking factor	BOEC	1.54	1.673	1.745	1.483	1.472	1.485	1.452
	EOEC		1.695	1.834	1.518	1.419	1.462	1.393
Peak Linear Power (kW/m)	Driver	30.14	33.1	32.4	30.1	27.4	25.1	26.8
	Internal Blanket	27.16	N/A	N/A	N/A	N/A	N/A	N/A
	Radial Blanket	17.76	N/A	N/A	N/A	N/A	N/A	N/A
Minimum Power to Melt at Centerline		150%	112%	113%	117%	123%	128%	117%
Average coolant flow rate (kg/s-pin)		N/A	0.15	0.15	0.15	0.13	0.13	0.13

4.3.2. Core Performance

The core performance for the equilibrium core with recycle is summarized in Table 4.8 and Table 4.9. These tables provide the charge enrichment (TRU volume fraction of heavy metal), fuel residence time, average and peak discharge burnups, the peak fast fluence for the inner core (IC), middle core (IC), and outer core (IC), the equilibrium loading, cycle length in effective full power days (EFPD), TRU consumption rate, and charge rates.

As discussed, the cycle length was a tradeoff between more control rods and shorter cycles. As the conversion ratio is reduced, the cycle length was reduced from approximately 1.7 and 1.0 years for the oxide and metal compact breakeven designs (longer for the blanket-free) to approximately four months for the zero conversion ratio designs. The fuel residence time does not vary widely with conversion ratio. Therefore, the fuel residence time measured by the number of cycles (batches) increases as a result of the shorter cycle length.

The fuel residence time in cycles is the number of batches in each region of the core. For batches with a non-integer value, some fraction of the assemblies will reside for different numbers of cycles and the value is the assembly-weighted average. This is a result of the flux gradient in the core, which may permit the fuel assemblies in outer rings to remain in the core for an additional cycle without exceeding fast fluence limits.

The peak fast fluence limit was 4.0×10^{23} n/cm^2 and most batches have a peak fluence close to this value. Maximizing the peak fast fluence will maximize fuel utilization as measured by the average discharge burnup.

The charge rate in kg per effective full power year is determined by the energy generated per unit mass. The heavy metal charge rate is determined by the traditional burnup (energy per unit mass HM), while the TRU charge rate is determined by the energy generated per unit mass of the TRU component of the heavy metal. As the conversion ratio is reduced, the burnup increases substantially, but the energy generated per unit mass of TRU declines, which leads to a nearly doubling of the TRU charge rate for the fertile-free (CR=0) relative to the breakeven (CR=1) cases. At high conversion ratios, the charge rate for the oxide is lower than the metal-fueled cases, but the values are very similar at very low conversion ratios.

Table 4.8 Cycle Performance Characteristics of Equilibrium Metal-Fueled ABR Cores

		S-PRISM	Blanket-free	Compact Core				
Conversion Ratio		N/A	1.00	1.00	0.75	0.50	0.25	0.00
Charge Enrichment, TRU/HM (v/f)	IC	N/A	10.7%	10.7%	16.1%	27.3%	46.2%	98.8%
	MC		13.4%	13.3%	20.2%	34.1%	57.8%	98.8%
	OC		16.1%	16.0%	24.2%	40.9%	69.3%	98.8%
Fuel residence time, cycles	IC	3	3	3	6	6	7	9
	MC		3	3	6	6	7	10
	OC		3.8	4.5	6.5	7	8	11
Burnup, MWd/kg	Ave. Driver	106.0	79.7	73.0	99.6	131.9	171.7	293.9
	Peak Driver	149.0	116.1	100.8	127.4	177.3	224.9	373.4
Peak Fast Fluence, 10^{23} n/cm^2	IC	3.71	3.84	4.00	3.86	4.00	4.00	4.00
	MC		3.80	3.77	4.00	3.96	3.70	3.92
	OC		4.00	3.68	3.97	3.75	2.92	3.77
	Blanket	3.90	N/A	N/A	N/A	N/A	N/A	N/A
Heavy Metal Loading, kg		26,092	23,556	16,749	13,436	9,449	5,920	3,623
TRU Loading, kg		3,078	3,518	2,447	2,856	3,084	3,242	3,567
Fissile Pu Loading, kg		2,336	2,320	1,643	1,535	1,348	1,157	1,056
Cycle Length, EFPD		595	596	370	232	221	158	132
TRU Consumption Rate, kg/EFPY		-33.6	-3.8	-4.7	83.1	173.8	272.8	376.0
TRU Charge, kg/EFPY		N/A	631	672	754	894	1,153	1,187
HM Charge, kg/EFPY		N/A	4,431	4,847	3,555	2,683	2,061	1,204

Table 4.9 Cycle Performance Characteristics of Equilibrium Oxide-Fueled ABR Cores

		S-PRISM	Blanket-free	Compact Core				
Conversion Ratio		N/A	1.00	1.00	0.75	0.50	0.25	0.00
Charge Enrichment, TRU/HM (v/f)	IC	N/A	13.8%	13.0%	21.3%	32.3%	50.7%	99.4%
	MC		17.2%	16.3%	26.6%	40.4%	63.4%	99.4%
	OC		20.7%	19.5%	32.0%	48.4%	76.1%	99.4%
Fuel residence time, cycles	IC	3	4	3	6	6	11	11
	MC		4	3	6	6	11	11
	OC		4	4.5	7	7	12	12
Burnup, MWd/kg	Ave. Driver	116.0	98.8	102.6	130.9	166.0	229.1	293.7
	Peak Driver	178.0	136.6	147.2	193.3	256.5	344.7	371.4
Peak Fast Fluence, 10^{23} n/cm^2	IC	2.96	3.99	4.00	4.00	3.91	4.00	4.00
	MC		4.00	3.84	3.87	3.88	4.00	3.24
	OC		2.84	3.82	3.91	4.00	3.91	2.98
	Blanket	2.44	N/A	N/A	N/A	N/A	N/A	N/A
Heavy Metal Loading, kg		34,926	32,841	19,284	15,253	10,910	6,865	3,913
TRU Loading, kg		5,208	6,121	3,490	3,884	4,081	4,002	3,880
Fissile Pu Loading, kg		3,469	3,591	2,109	1,937	1,695	1,400	1,128
Cycle Length, EFPD		621	874	607	353	326	165	124
TRU Consumption Rate, kg/EFPY		-38.6	-5.6	-7.1	83.1	177.6	274.2	377.4
TRU Charge, kg/EFPY		N/A	633	582	676	808	924	1,196
HM Charge, kg/EFPY		N/A	3,571	3,440	2,700	2,129	1,542	1,204

Figure 4.6 shows the core average charge density of heavy metal and TRU for the metal and oxide-fueled cores. There is a slight increase in the TRU charge density at lower conversion ratios, while the heavy metal charge density decreases dramatically as the conversion ratio is reduced. The metal-fueled core requires slightly a higher heavy metal charge concentrations, while the oxide fueled core requires a slightly higher TRU charge concentration. The difference is most significant at high conversion ratios and switches at very low conversion ratios.

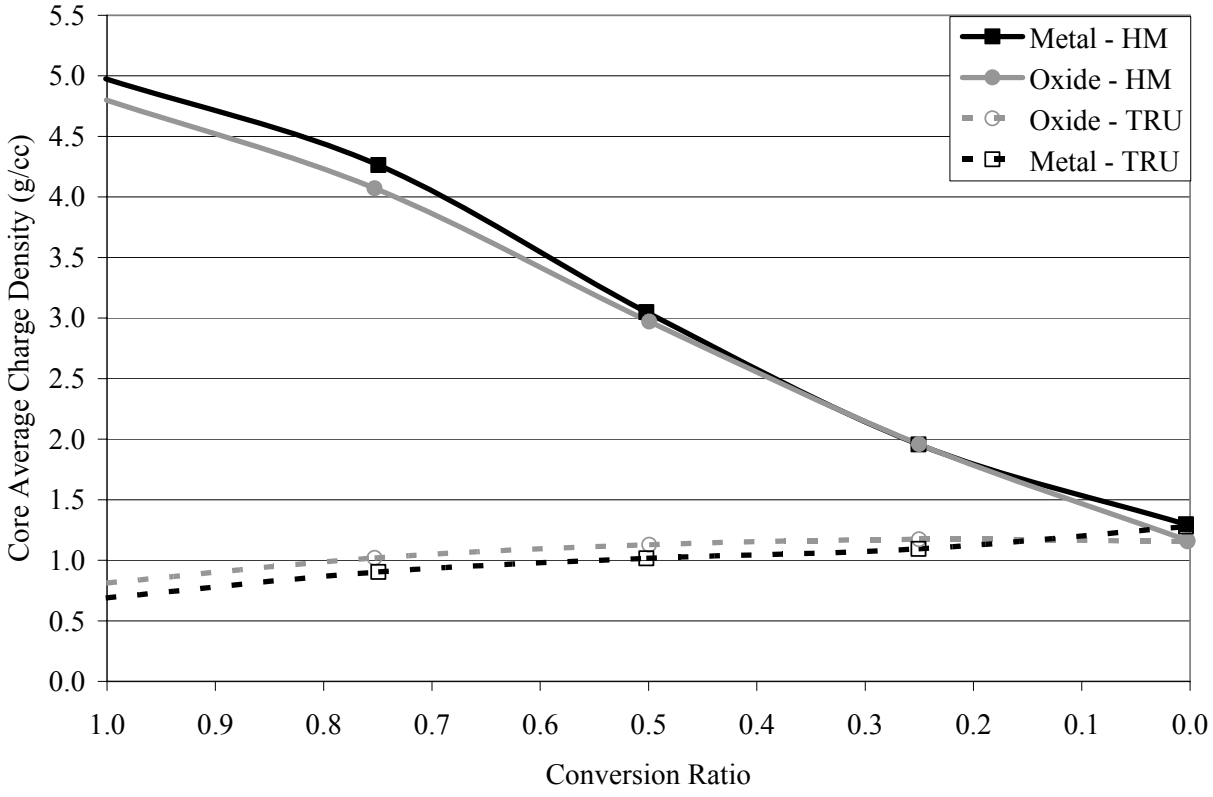

Figure 4.6 Charge Density Dependence on Conversion Ratio

Figure 4.7 shows the core average charge enrichment TRU / HM for the metal and oxide-fueled cores. The differences in neutron spectra between the metal and oxide-fueled cores result in the oxide core having a slightly higher enrichment for a given conversion ratio. Regardless of the design, to have a true conversion ratio of zero, a uranium free fuel form is required. The significance of this curve is that if an enrichment limit were imposed on the fuel, this would impose a limit on the conversion ratio which would be significantly higher for the oxide core than the metal-fueled core for a given enrichment.

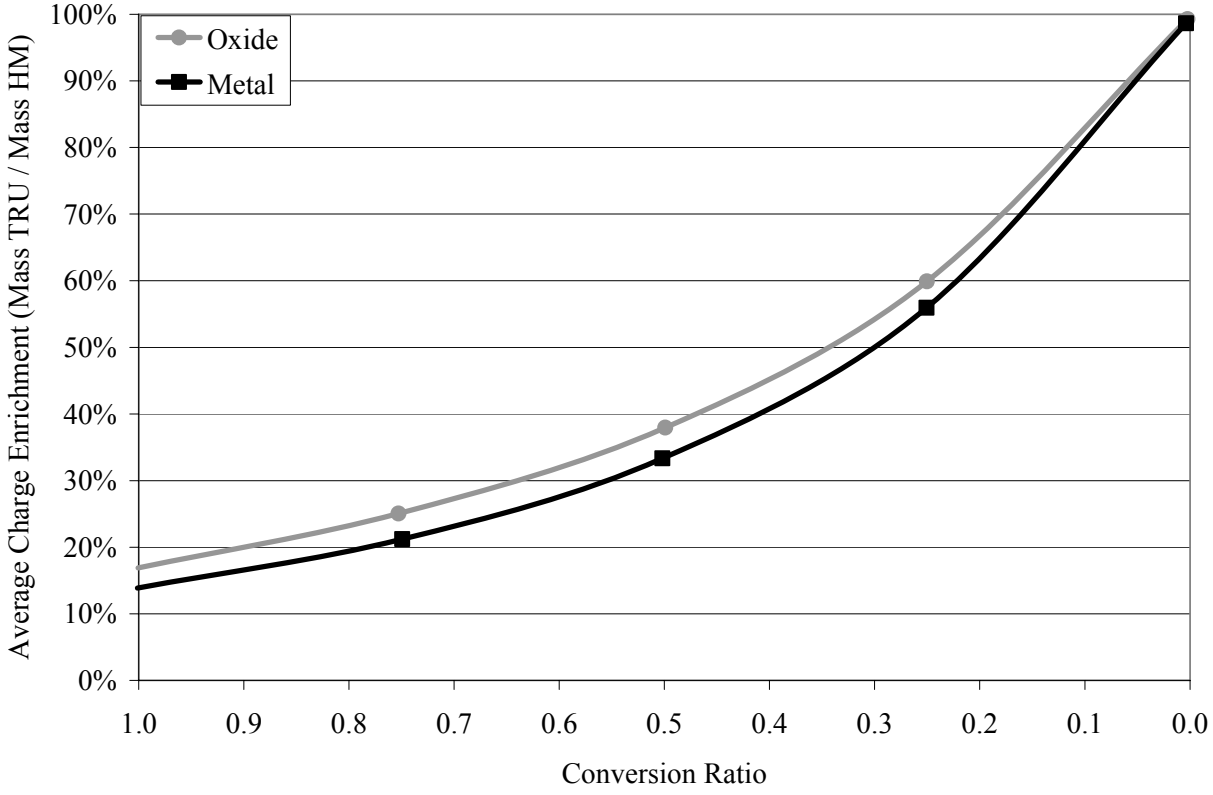

Figure 4.7 Enrichment Dependence on Conversion Ratio

4.4. Systems Performance Data

The dynamic and equilibrium state of the GNEP system will be highly dependent on the performance of the ABR at equilibrium (steady-state) conditions and during the transition from the initial core loadings to the equilibrium conditions. An effort was made to quantify a number of parameters which are important to the sizing and deployment of the various major components of the GNEP system, which includes the LWRs, ABRs, and fuel cycle facilities. The relative number of LWR to ABR is primarily determined by the conversion ratio.

The previous analyses focused on the performance of the ABR at equilibrium conditions with recycle of the spent ABR fuel with LWR spent fuel used only for makeup TRU feed. However, the initial ABR cores will most likely be fueled solely by TRU recovered from LWR spent fuel and operated using this material until the fast reactor fuel can be reprocessed and made available to manufacture new fuel. The calculations were performed using the same design, cycle lengths, and fuel batches as the equilibrium core. This means that the conversion ratio is allowed to float and the design has not been optimized for fast fluence and/or linear power. The objective was to provide an estimate of the performance of the initial cycles and the transition to equilibrium. Table 4.10 provides the summary data for HM and TRU mass balances that would be used in the system analyses.

Table 4.10 Mass Balance of Startup and Equilibrium ABR Cores

	Metal					Oxide				
Equilibrium Core										
Conversion Ratio	1.00	0.75	0.50	0.25	0.00	1.00	0.75	0.50	0.25	0.00
HM Inventory (kg TRU / MWt)	16.75	13.44	9.45	6.17	3.62	19.28	15.25	10.91	6.86	3.91
TRU Inventory (kg TRU / MWt)	2.45	2.86	3.08	3.36	3.57	3.49	3.88	4.08	4.00	3.88
HM Makeup Feed Rate (kg/MWt-yr)	0.38	0.39	0.39	0.38	0.39	0.39	0.39	0.39	0.39	0.39
TRU Makeup Feed Rate (kg/MWt-yr)	-0.02	0.08	0.18	0.29	0.40	0.00	0.07	0.16	0.26	0.36
Startup Core										
Conversion Ratio	0.97	0.75	0.53	0.31	0.08	0.97	0.76	0.54	0.32	0.11
HM Inventory (kg TRU / MWt)	16.75	13.43	9.44	5.91	3.61	19.28	15.24	10.90	6.85	3.90
TRU Inventory (kg TRU / MWt)	2.67	2.76	2.70	2.60	2.71	3.61	3.64	3.53	3.25	2.96
HM Makeup Feed Rate (kg/MWt-yr)	0.38	0.39	0.39	0.39	0.39	0.39	0.39	0.39	0.39	0.39
Makeup Feed Rate (kg TRU / MWt-yr)	0.00	0.07	0.16	0.26	0.36	0.00	0.08	0.17	0.26	0.35
Additional TRU Inventory for Equilibrium (kg TRU / MWt)	-0.22	0.10	0.38	0.76	0.85	-0.12	0.25	0.55	0.76	0.92

Figure 4.8 compares the conversion ratio for the equilibrium core with the same core design during startup. The startup core will have a slightly lower conversion ratio at high conversion ratio and a significantly higher conversion ratio at very low conversion ratio. This means that a lower fuel volume fraction would be required for the startup fuel than would be required at equilibrium for a given conversion ratio. The more dominant factor in determining the conversion ratio of the startup core will likely be the management of the existing LWR spent fuel inventory based on the deployment rate of ABRs. All conversion ratios require similar levels of TRU to startup, but very large differences in makeup feed are required at different conversion ratios.

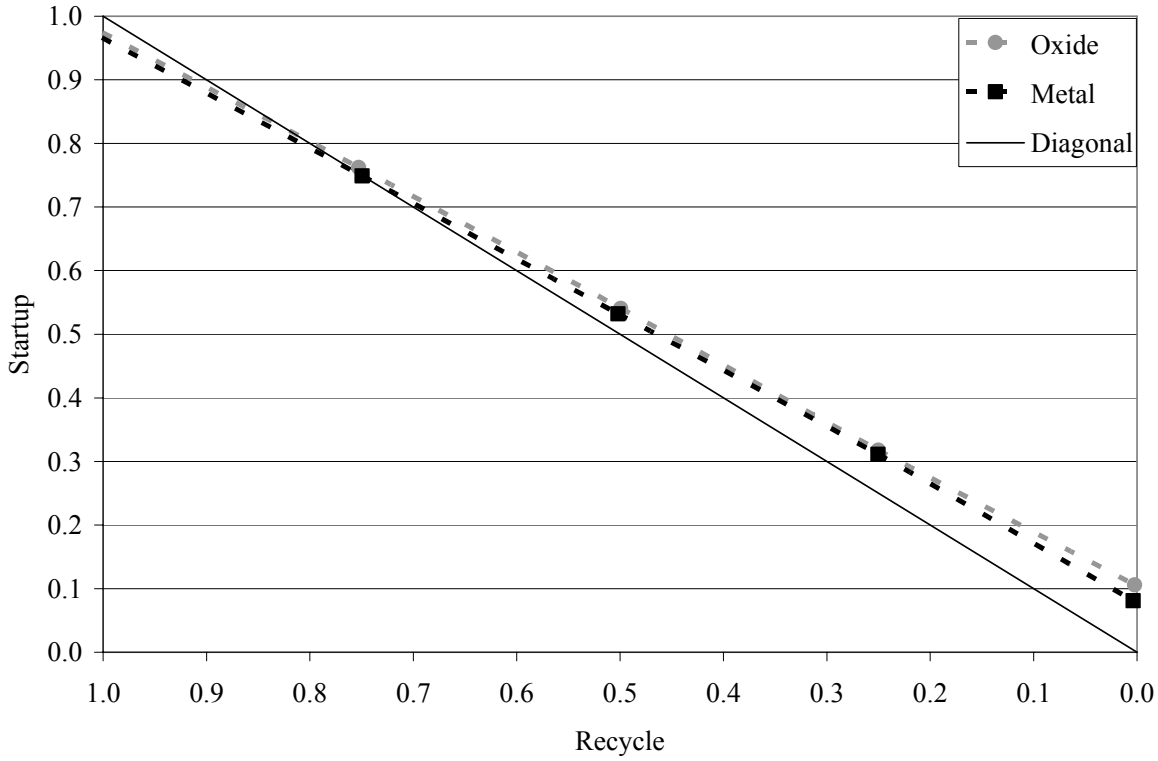

Figure 4.8 Startup and Equilibrium Core Conversion Ratio for a Fixed Configuration

Figure 4.9 provides the equilibrium and startup ABR in-core inventory normalized by the thermal power. The TRU inventory is relatively insensitive (≤20% variation) to the conversion ratio, with the exception of the equilibrium metal-fueled core which has a 46% increase in in-core TRU inventory from breakeven to fertile-free.

The shift in the isotopic composition between startup and equilibrium will change the required in-core TRU inventory. The TRU inventory in the startup core is less than the equilibrium core, except at conversion ratios near 1.0. The required in-core TRU inventory will slowly shift from startup levels to equilibrium levels as the fuel is recycled back into the core, but the actual behavior was not modeled in this study. During the transition from startup to equilibrium, the external supply of TRU will be required to both replace the TRU that was destroyed and compensate for the shift in in-core TRU inventory.

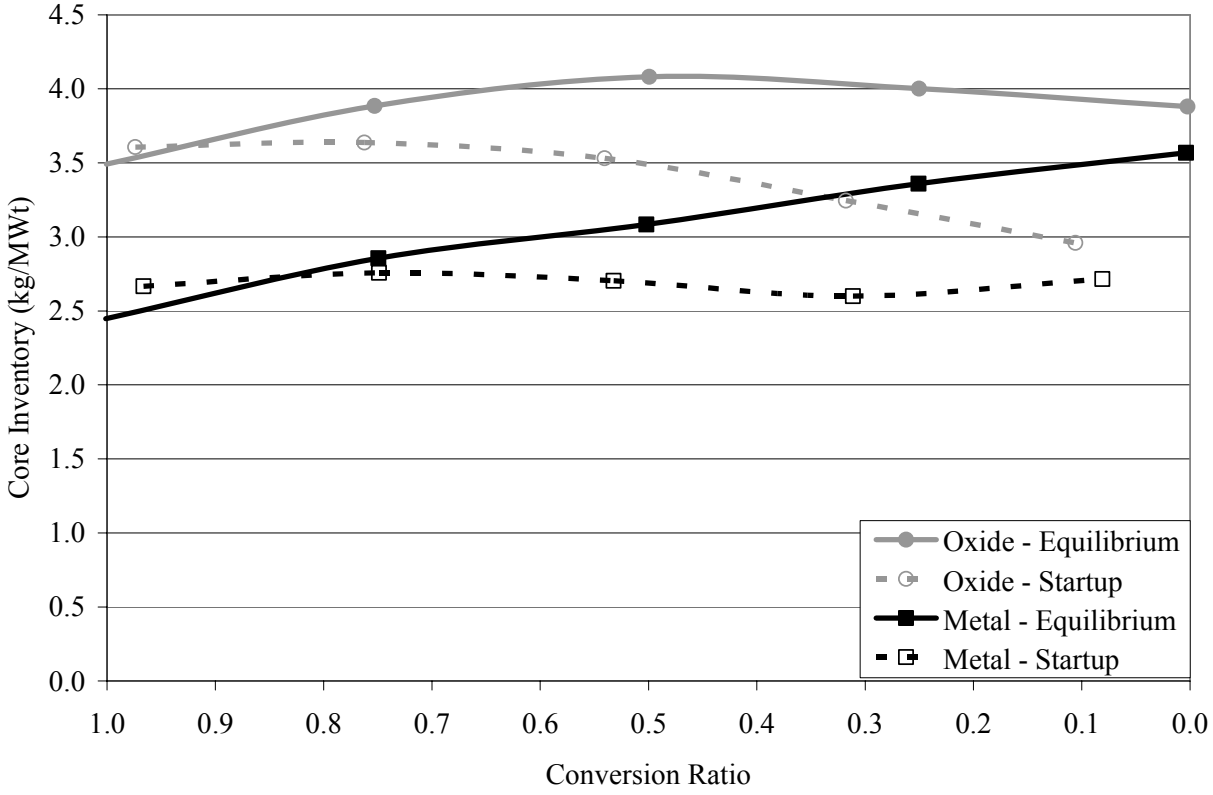

Figure 4.9 Specific Reactor Loading Dependence of ABR on Conversion Ratio

Figure 4.10 shows the TRU destruction rate as a function of conversion ratio. The total heavy metal destruction rate is approximately 0.4 kg/MWt-yr and the fraction which results from the net destruction of TRU (TRU fission minus TRU production) is the amount of makeup TRU that must be provided from the recycle of LWR spent fuel. The value doesn't go exactly to zero at a conversion ratio of 1.0 because of the definition of TRU conversion ratio. The TRU destruction value was calculated based on mass charged and mass present at 5 years cooling, which gives a slightly different result. A small additional quantity will be needed to compensate for losses to the waste stream.

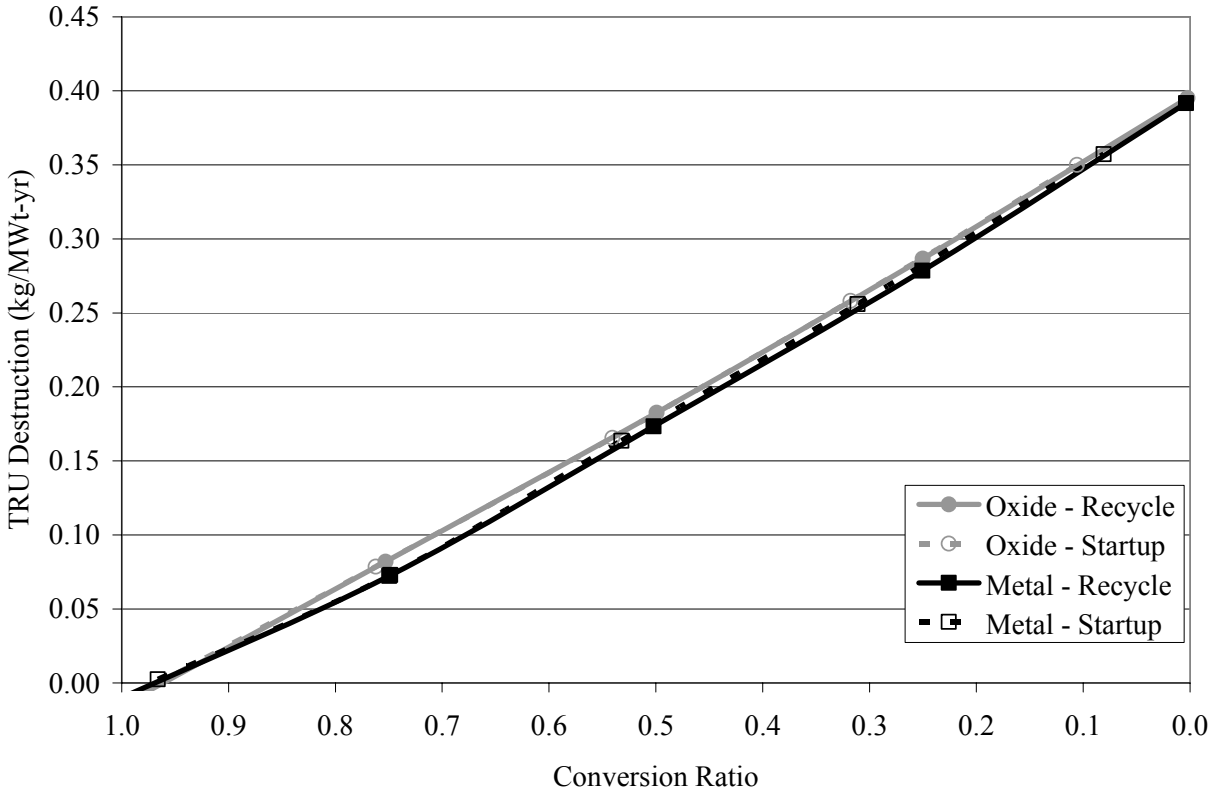

Figure 4.10 Transuranic Destruction Rate Dependence on Conversion Ratio

Figure 4.11 shows the reprocessing rate of different fuel types for the startup and recycle cases. The startup assumes no recycle of fast reactor fuel. This provides an approximation of the LWR processing rate that will be required until the TRU from the recycled fast reactor is available. At equilibrium, the LWR spent fuel reprocessing rate will decline to the level required for. The total reprocessing rate of spent fuel (kg initial heavy metal) is much higher for the startup cores because of the very low concentration of TRU in the LWR spent fuel. This also shows that much greater LWR SNF reprocessing capacity must exist to supply the initial startup core and operate the reactor until the fast reactor fuel can be recycled. This LWR SNF reprocessing capacity must be used to start new ABRs or there will be a large amount of excess capacity after steady state operation begins. The LWR SNF reprocessing capacity is very important consideration early in the deployment phase of the GNEP system. The reprocessing requirements for the equilibrium core increase rapidly at lower conversion ratios because of the increased requirement for LWR makeup feed which has a significantly lower concentration of TRU, which requires a great mass of heavy metal to be processed to produce the same quantity of TRU to be used in the fresh fuel. However, the primary mission of the ABR is to consume the TRU from LWR SNF and a high processing rate is likely a benefit as long as sufficient reprocessing capacity exists to fuel new ABRs and provide makeup for existing ABRs.

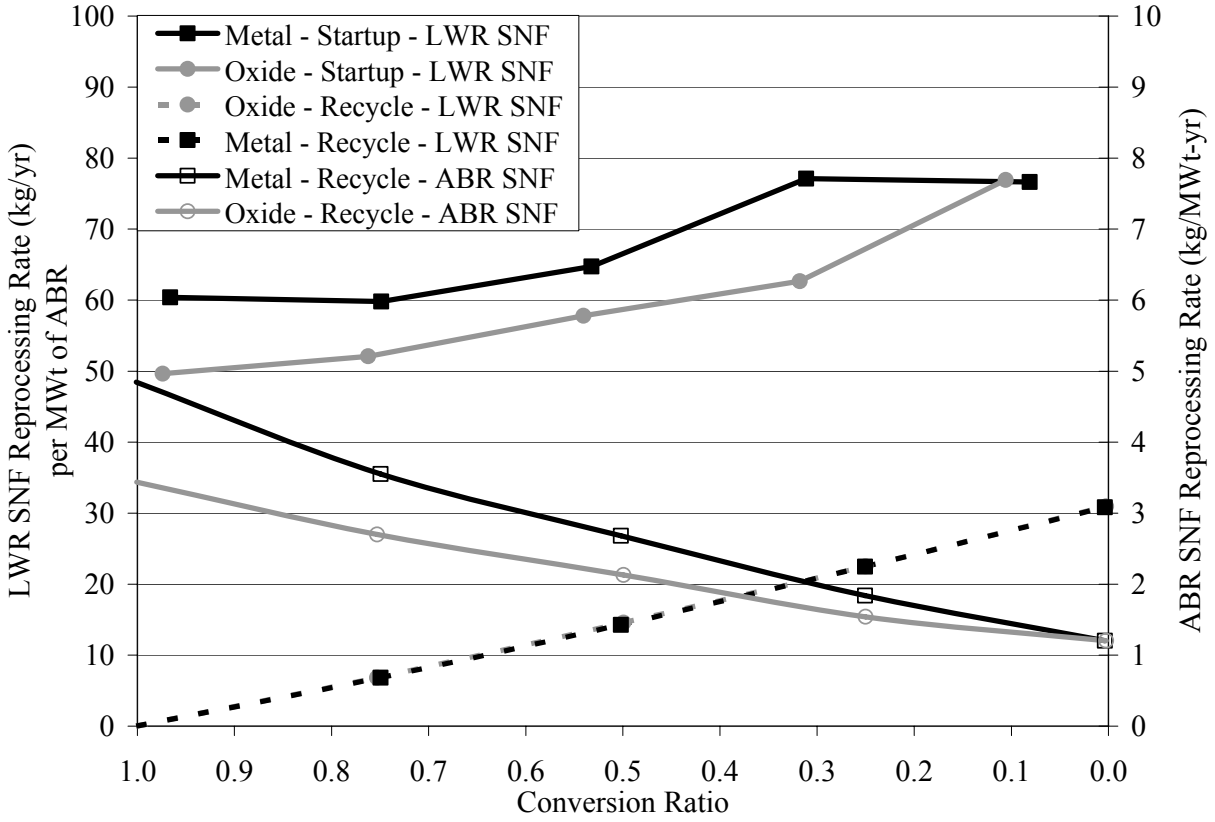

Figure 4.11 Spent Nuclear Fuel Reprocessing Rate Dependence on Conversion Ratio

Figure 4.12 provides the fractional destruction of TRU in a single pass through the ABR. This is not only highly sensitive to conversion ratio, but becomes increasingly sensitive to discharge burnup at low conversion ratios. The discharge burnup was assumed to be limited only by fast fluence on the cladding and the same value was assumed for metal and oxide. The softer spectrum in the oxide-fueled cores results in a higher average discharge burnup at all but the lowest conversion ratios. The fraction of TRU that ultimately ends up in the waste stream is determined primarily by the efficiency of the reprocessing system. However, if a greater fraction is destroyed in a given pass, the effective number of times the material is recycled is reduced and therefore the fraction that ends up in the waste stream is reduced for a given reprocessing efficiency. For the breakeven core, the TRU would be retained in the cycle indefinitely, while at very low conversion ratios as much as 30% or more of the TRU can be destroyed in a single pass. The oxide fuel seems to be able to destroy a slightly greater fraction of the TRU in a single pass at medium conversion ratios because of the higher average discharge burnup.

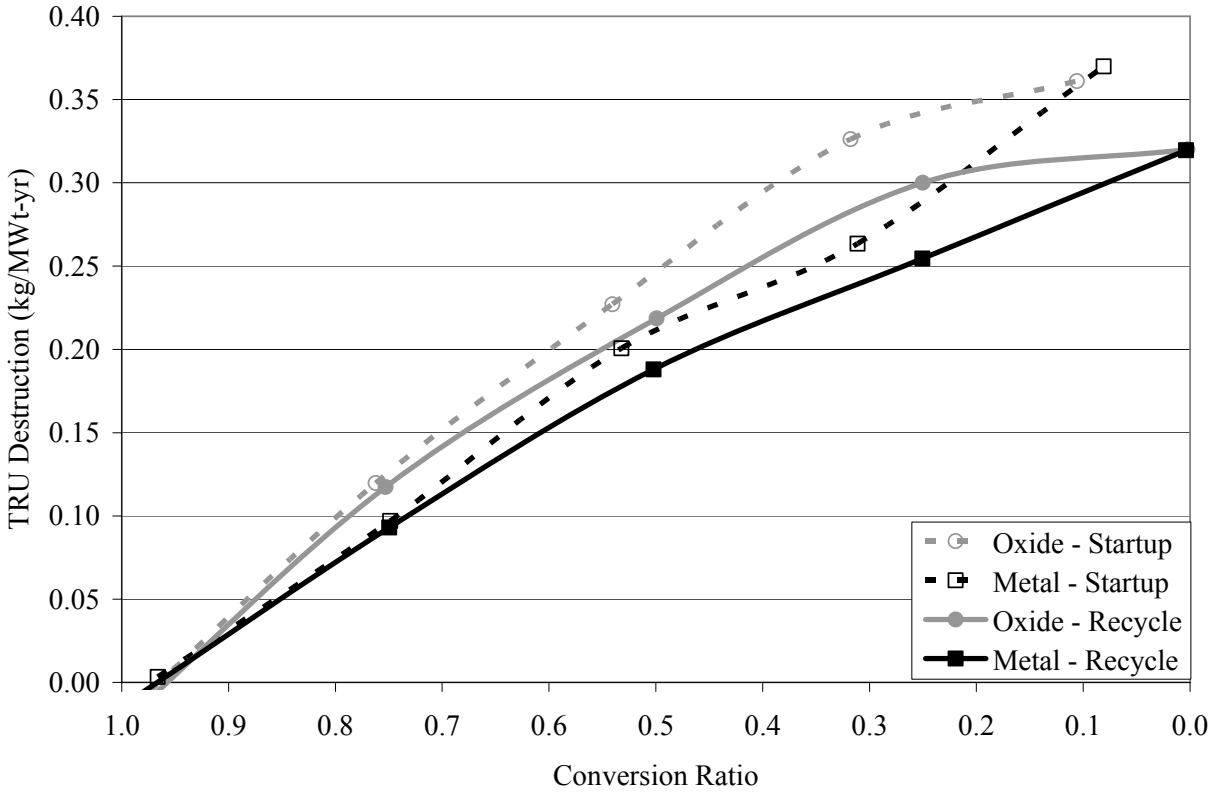

Figure 4.12 Fractional Destruction Rate Dependence on Conversion Ratio

4.5. Alternative Fuel Cycle for CR=0.5 Configuration

The reference ABR TRU feed was based on the recycle of ALWR SNF. A variety of other feed streams based on a single recycle of either the plutonium or plutonium and neptunium and the separation of curium for additional decay prior to being used in the fuel manufacturing. The GNEP scenarios assumed that the spent UOX fuel was reprocessed at 5 years and all TRU was recovered and used as the makeup feed for fast reactors. The reference UOX fuel a standard 17x17 PWR assembly loaded with enriched uranium and irradiated to 50 MWd/kg. The composition of the TRU makeup feed stream for the equilibrium state are provided in Table 4.11.

Table 4.11 TRU Composition (w/o) of External Feed to ABR

	Ref. LWR (50GWd5yr)	1B	2A	2B	2C1	2C2	30GWd30yr
U-234	0.000	0.000	0.000	0.000	0.000	0.000	0.000
U-235	0.000	0.000	0.000	0.000	0.000	0.000	0.000
U-236	0.000	0.000	0.000	0.000	0.002	0.000	0.000
U-238	0.000	0.000	0.000	0.000	0.000	0.000	0.000
NP237	4.777	7.066	4.303	3.810	3.810	4.794	3.777
PU236	0.000	0.000	0.000	0.000	0.000	0.000	0.000
PU238	2.310	3.540	5.986	5.170	5.171	2.366	0.981
PU239	47.899	24.045	40.457	34.947	34.957	47.476	53.046
PU240	22.510	28.835	28.140	24.582	25.237	22.852	23.530
PU241	10.580	11.844	11.380	9.829	9.831	10.663	3.016
PU242	6.519	9.028	9.734	8.407	8.408	6.665	4.957
AM241	3.356	9.412	0.000	8.359	8.360	3.383	9.773
AM242	0.006	0.052	0.000	0.049	0.049	0.006	0.003
AM243	1.475	4.790	0.000	3.579	3.580	1.532	0.829
CM242	0.000	0.000	0.000	0.000	0.000	0.000	0.000
CM243	0.005	0.013	0.000	0.014	0.008	0.003	0.001
CM244	0.515	1.239	0.000	1.079	0.414	0.210	0.074
CM245	0.041	0.123	0.000	0.161	0.160	0.044	0.011
CM246	0.005	0.012	0.000	0.012	0.012	0.006	0.001

The COEX (1B) scenario assumed that the Pu was separated from the spent UOX fuel and then irradiated a single time as MOX fuel in an LWR under the same conditions as the original UOX fuel. After five years of storage, the spent MOX fuel is then processed and all TRU isotopes are recovered and blended with the bypass Np, Am, and Cm from the spent UOX fuel to provide the makeup feed for the fast reactors. The bypass feed stream was assumed to be stored for an additional 15 years, which is the approximate time to produce, irradiate, cool, and reprocess the MOX fuel.

The UREX+2 (2A) scenario assumed that the Np and Pu were separated from the spent UOX fuel and then irradiated a single time as MOX fuel in an LWR under the same conditions as the original UOX fuel. After five years of storage, the spent MOX fuel is then processed using the same technology, which would recover only the Np and Am to provide the makeup feed for the fast reactors. The spent fast reactor fuel was assumed to recycle all TRU isotopes back into the fast reactor. All Am and Cm from reprocessing the LWR fuel are assumed to be sent to waste.

The UREX+3 (2B) scenario assumed that the Np and Pu were separated from the spent UOX fuel and then irradiated a single time as MOX fuel in an LWR under the same conditions as the original UOX fuel. After five years of storage, the spent MOX fuel is then processed and all TRU isotopes are recovered and blended with the bypass Am and Cm from the spent UOX fuel to provide the makeup feed for the fast reactors. The bypass feed stream was assumed to be stored for an additional 15 years, which is the approximate time to produce, irradiate, cool, and reprocess the MOX fuel.

The UREX+4 (2C1) scenario assumed that the Np and Pu were separated from the spent UOX fuel and then irradiated a single time as MOX fuel in an LWR under the same conditions as the original UOX fuel. After five years of storage, the spent MOX fuel is then processed and all Np, Pu, and Am isotopes are recovered and blended with the bypass Am and Cm from the spent UOX fuel to provide the makeup feed for the fast reactors. The Cm recovered from the recycled MOX is allowed to decay for an addition 25 years prior to being blended into the TRU makeup feed. The Am and Cm from the spent UOX fuel in the bypass feed stream are assumed to be separated and stored for an additional 15 years and 40 years respectively. The spent fast reactor fuel was assumed to recycle all TRU isotopes back into the fast reactor. The additional 25 years of storage is to allow the Cm additional decay time to reduce the radiological hazard associated with Cm recycle.

The UREX+4 (2C2) scenario is the same as the previous scenario except the single recycle as MOX in the LWR is not performed and the Np, Pu, and Am from the 5 year cooled spent UOX fuel are used as TRU makeup feed for the fast reactor. The Cm from the spent UOX is allowed to decay for an additional 25 years before being used as TRU makeup feed. The spent fast reactor fuel was assumed to recycle all TRU isotopes back into the fast reactor.

The 30GWd30yr is the same as the reference fuel cycle except the LWR SNF was irradiated to 30 GWd/MT and cooled for 30 years prior to reprocessing. The calculations were done for the startup cycle without recycle of the fast reactor fuel. This feed is more representative of the current inventory of SNF in storage. Over time, the feed stream will likely transition from this feed to the reference feed or the existing spent fuel could be blended with new spent fuel in order to use the backlog of SNF that will exist when the ABRs are initially deployed.

The impact on the performance of the metal and oxide CR=0.5 designs were evaluated for these different feed streams. The design, and external cycle for the fast reactor remained unchanged except a different make TRU feed stream was used. Figure 4.13 shows the conversion ratio for the CR=0.5 design with different feed streams. There is very little impact on the equilibrium ABR conversion ratio over this range of feed streams. Case 1B has the largest reduction in fissile plutonium in the feed stream. For the Case 1B external feed, the equilibrium conversion ratio would be reduce to approximately 0.45 and the TRU enrichment increased by approximately 5% relative to the reference ABR designs. This would require a small increase in fuel volume fraction in order to achieve the target CR if the equilibrium GNEP scenario would include a single pass of the plutonium in an LWR. The results show that for a wide range of

single pass MOX there is little impact on the equilibrium design of the ABR. Additionally, separation and storage of curium has essentially no impact on the ABR.

Most other parameters showed little significant change. The designs were not modified to achieve the target conversion ratio or optimized to the fluence limit. However, the fluence changed only slightly (less than 10%). This all suggests that the ABR should have sufficient flexibility to operate with a wide range of TRU feeds for different LWR operation scenarios with a single-pass MOX with little effect on the ABR performance. The use of single-pass MOX would reduce the ratio of fast reactor to light-water reactors in the system, which is desirable if the fast reactors prove to be more expensive than the LWRs.

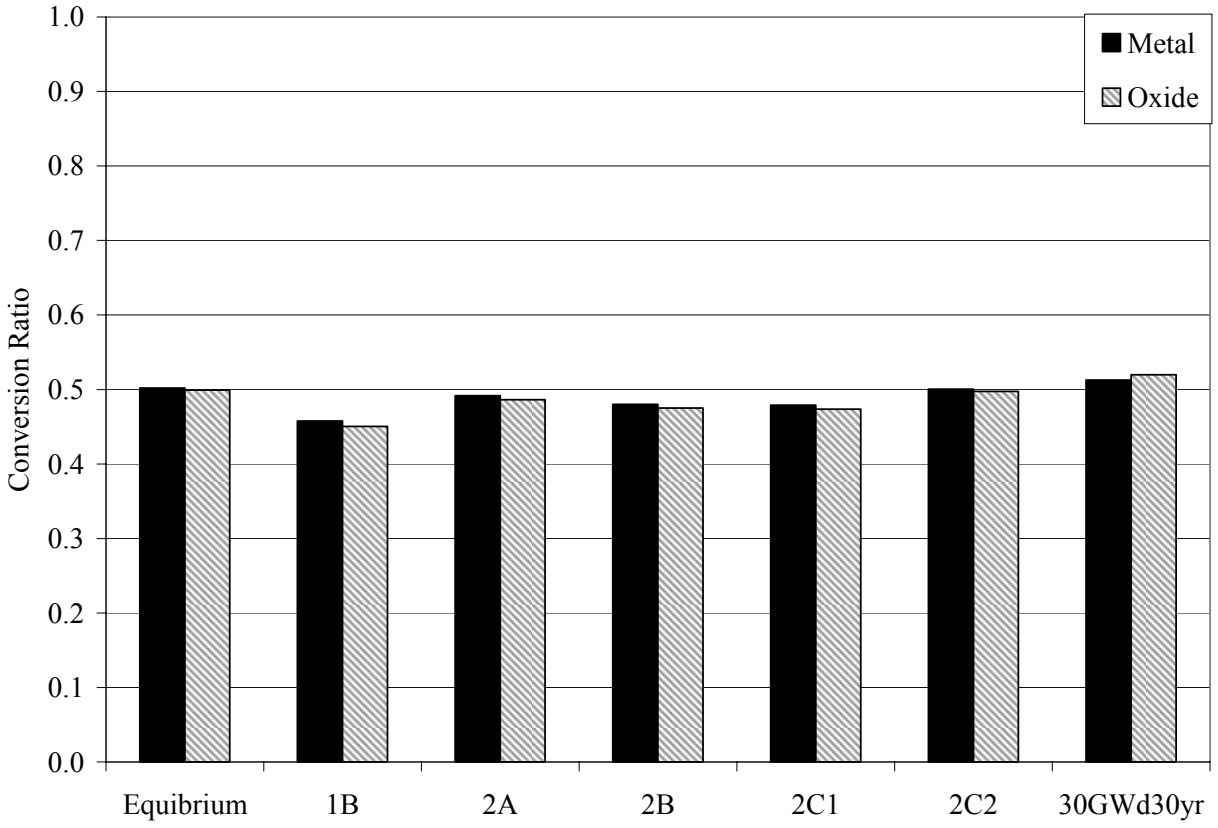

Figure 4.13 Equilibrium Conversion Ratio with Different TRU Feed Streams

4.6. Systems Data Summary

Detailed systems data, including detailed isotopic data, was calculated for the equilibrium and startup fuel cycle all the ABR designs evaluated. This same data was generated for the other fuel cycles that were analyzed. This section provides a summary of the systems data. The charge and five-year cooled data for the equilibrium fuel cycle for the metal-fueled ABR are provided in Table 4.12 and Table 4.13. The charge and five-year cooled data for the equilibrium fuel cycle for the oxide-fueled ABR are provided in Table 4.14 and Table 4.15. The charge and five-year cooled data for the startup fuel cycle for the metal-fueled ABR are provided in Table 4.16 and Table 4.17. The charge and five-year cooled data for the startup fuel cycle for the oxide-fueled ABR are provided in Table 4.18 and Table 4.19.

The inventory of the metal-fueled core is lower than the oxide-fueled core for both heavy metal and TRU, which is part due to the shorter active core height. The metal-fueled core TRU inventory is approximately 30% lower for the breakeven core and 8% lower for the fertile-free core than the equivalent oxide-fueled core at equilibrium. For the high conversion ratio designs, the metal-fueled designs will have a significantly lower fraction of higher actinides. There is very little difference in the composition of the fuel at very low conversion ratios.

Table 4.12 Charge Data for the Equilibrium Fuel Cycle for Metal-Fueled ABR

Reference Conversion Ratio	1.00	0.75	0.50	0.25	0.00
Actual Conversion Ratio	1.00	0.75	0.50	0.25	0.00
Heavy Metal (g/MTIHM)	1,000,000	999,900	999,900	1,000,000	1,000,000
Plutonium (g/MTIHM)	134,220	194,900	295,310	482,500	832,000
Neptunium (g/MTIHM)	879	3,341	7,122	14,103	27,663
Americium (g/MTIHM)	2,878	10,045	21,261	42,159	81,670
Curium (g/MTIHM)	694	3,845	9,597	21,286	44,955
U-235 (g/MTIHM)	355	427	509	645	841
Pu-238 (g/MTIHM)	1,501	5,183	11,102	22,316	43,744
Pu-239 (g/MTIHM)	88,628	103,630	128,610	174,460	258,260
Pu-240 (g/MTIHM)	36,610	61,603	102,590	178,570	318,440
Pu-241 (g/MTIHM)	4,430	10,752	21,640	42,234	82,260
Am-241 (g/MTIHM)	1,921	5,373	10,541	19,954	37,399
U-235/U	0.04%	0.05%	0.08%	0.15%	6.13%
TRU/HM	13.9%	21.2%	33.3%	56.0%	98.6%
BOEC HM (kg)	16,749	13,436	9,449	6,169	3,623
BOEC TRU (kg)	2,447	2,856	3,084	3,359	3,567
Reprocessed TRU Feed Rate[1] (kg/year)	571	570	612	667	689
Makeup TRU Feed Rate[1] (kg/year)	0	71	148	233	320
HM Charge Rate[1] (kg/year)	4,117	3,020	2,279	1,608	1,022

[1]Assumes 85% capacity factor

Table 4.13 Five-Year Cooled Data for the Equilibrium Fuel Cycle for Metal-Fueled ABR

Reference Conversion Ratio	1.00	0.75	0.50	0.25	0.00
Average Discharge Burnup, GWd/MTIHM	73.0	99.6	131.9	186.9	293.9
Heavy Metal (g/MTIHM)	923,400	893,200	859,500	803,100	685,700
Plutonium (g/MTIHM)	135,550	176,530	237,610	351,810	544,600
Neptunium (g/MTIHM)	870	2,090	3,926	7,121	12,676
Americium (g/MTIHM)	3,711	10,320	20,625	39,769	74,490
Curium (g/MTIHM)	616	3,466	8,469	18,829	39,409
Fission Products (g/MTIHM)	74,840	99,730	124,500	164,950	246,140
U-235 (g/MTIHM)	210	273	375	559	875
Pu-238 (g/MTIHM)	1,515	4,759	9,733	19,234	36,547
Pu-239 (g/MTIHM)	90,010	94,100	98,110	104,670	106,250
Pu-240 (g/MTIHM)	37,267	58,288	90,200	149,730	252,390
Pu-241 (g/MTIHM)	3,667	7,019	12,234	22,284	40,346
Am-241 (g/MTIHM)	2,758	6,002	10,904	19,758	35,217
Sr-90 (g/MTIHM)	532	684	828	1,049	1,486
Y-90 (g/MTIHM)	0.13	0.17	0.21	0.26	0.37
Cs-137 (g/MTIHM)	2,463	3,286	4,122	5,488	8,226
Ba-137 (g/MTIHM)	441	606	753	997	1,503
U-235/U	0.03%	0.04%	0.06%	0.14%	6.03%
TRU/HM	15.2%	21.5%	31.5%	52.0%	97.9%

Table 4.14 Charge Data for the Equilibrium Fuel Cycle for Oxide-Fueled ABR

Reference CR	1.00	0.75	0.50	0.25	0.00
Actual Conversion Ratio	1.00	0.75	0.50	0.25	0.00
Heavy Metal (g/MTIHM)	999,800	1,000,000	1,000,000	1,000,000	999,900
Plutonium (g/MTIHM)	161,750	228,280	334,150	514,900	836,800
Neptunium (g/MTIHM)	707	3,354	7,468	14,535	25,889
Americium (g/MTIHM)	5,045	13,012	25,027	44,560	80,080
Curium (g/MTIHM)	1,675	5,849	12,860	25,056	49,996
U-235 (g/MTIHM)	435	523	622	730	509
Pu-238 (g/MTIHM)	2,278	6,528	13,024	23,734	44,126
Pu-239 (g/MTIHM)	94,650	111,250	138,040	185,170	255,900
Pu-240 (g/MTIHM)	51,798	78,210	119,750	189,550	322,840
Pu-241 (g/MTIHM)	7,262	14,561	26,549	47,430	83,450
Am-241 (g/MTIHM)	3,182	6,988	12,471	21,218	36,243
U-235/U	0.05%	0.07%	0.10%	0.18%	7.14%
TRU/HM	16.9%	25.0%	38.0%	59.9%	99.3%
BOEC HM (kg)	19,284	15,253	10,910	6,865	3,913
BOEC TRU (kg)	3,490	3,884	4,081	4,002	3,880
Reprocessed TRU Feed Rate[1] (kg/year)	494	504	536	551	695
Makeup TRU Feed Rate[1] (kg/year)	0	71	151	233	321
HM Charge Rate[1] (kg/year)	2,922	2,294	1,809	1,310	1,023

[1]Assumes 85% capacity factor

Table 4.15 Five-Year Cooled Data for the Equilibrium Fuel Cycle for Oxide-Fueled ABR

Reference Conversion Ratio	1.00	0.75	0.50	0.25	0.00
Average Discharge Burnup, GWd/MTIHM	102.6	130.9	166.0	229.1	293.7
Heavy Metal (g/MTIHM)	890,400	858,900	820,800	752,400	684,200
Plutonium (g/MTIHM)	164,720	200,660	257,930	350,800	547,190
Neptunium (g/MTIHM)	708	1,776	3,296	5,699	11,046
Americium (g/MTIHM)	6,524	13,454	23,914	40,520	73,250
Curium (g/MTIHM)	1,531	5,213	11,425	22,310	43,612
Fission Products (g/MTIHM)	105,770	130,540	157,520	206,290	246,510
U-235 (g/MTIHM)	226	324	457	623	630
Pu-238 (g/MTIHM)	2,371	5,911	11,254	19,872	36,535
Pu-239 (g/MTIHM)	96,730	96,610	97,120	96,800	103,940
Pu-240 (g/MTIHM)	53,585	72,930	103,390	152,960	255,910
Pu-241 (g/MTIHM)	6,131	9,344	14,585	23,494	41,091
Am-241 (g/MTIHM)	4,652	7,930	12,672	19,925	34,448
Sr-90 (g/MTIHM)	712	858	1,004	1,270	1,472
Y-90 (g/MTIHM)	0.18	0.22	0.25	0.32	0.37
Cs-137 (g/MTIHM)	3,395	4,203	5,108	6,753	8,201
Ba-137 (g/MTIHM)	732	915	1,089	1,401	1,541
U-235/U	0.03%	0.05%	0.09%	0.19%	6.92%
TRU/HM	19.5%	25.7%	36.1%	55.7%	98.7%

Table 4.16 Charge Data for the Startup Fuel Cycle for Metal-Fueled ABR

Reference Conversion Ratio	1.00	0.75	0.50	0.25	0.00
Actual Conversion Ratio	0.97	0.75	0.53	0.31	0.08
Heavy Metal (g/MTIHM)	1,000,000	1,000,000	1,000,000	1,000,000	1,000,000
Plutonium (g/MTIHM)	136,660	184,430	264,630	410,300	698,400
Neptunium (g/MTIHM)	7,185	9,702	13,916	21,579	36,724
Americium (g/MTIHM)	7,419	10,015	14,371	22,282	37,921
Curium (g/MTIHM)	877	1,184	1,699	2,635	4,485
U-235 (g/MTIHM)	1,678	1,574	1,400	1,083	457
Pu-238 (g/MTIHM)	3,492	4,712	6,759	10,484	17,843
Pu-239 (g/MTIHM)	72,681	98,100	140,700	218,190	371,350
Pu-240 (g/MTIHM)	34,287	46,289	66,400	102,990	175,250
Pu-241 (g/MTIHM)	16,182	21,842	31,341	48,590	82,700
Am-241 (g/MTIHM)	5,133	6,930	9,944	15,417	26,237
U-235/U	0.20%	0.20%	0.20%	0.20%	0.21%
TRU/HM	15.2%	20.5%	29.5%	45.7%	77.8%
BOEC HM (kg)	16,747	13,432	9,443	5,914	3,613
BOEC TRU (kg)	2,667	2,756	2,704	2,600	2,715
Reprocessed TRU Feed Rate[1] (kg/year)	0	0	0	0	0
Makeup TRU Feed Rate[1] (kg/year)	626	620	671	800	795
HM Charge Rate[1] (kg/year)	4,117	3,020	2,279	1,751	1,022

[1]Assumes 85% capacity factor

Table 4.17 Five-Year Cooled Data for the Startup Fuel Cycle for Metal-Fueled ABR

Reference Conversion Ratio	1.00	0.75	0.50	0.25	0.00
Average Discharge Burnup, GWd/MTIHM	73.0	99.6	131.9	171.7	294.1
Heavy Metal (g/MTIHM)	923,400	894,300	859,100	818,700	685,200
Plutonium (g/MTIHM)	136,960	166,780	209,630	295,850	426,060
Neptunium (g/MTIHM)	4,544	5,368	7,241	11,598	16,289
Americium (g/MTIHM)	9,037	11,635	16,196	25,281	40,397
Curium (g/MTIHM)	1,100	1,655	2,447	3,720	7,241
Fission Products (g/MTIHM)	71,949	98,670	130,050	165,620	283,730
U-235 (g/MTIHM)	833	690	596	505	260
Pu-238 (g/MTIHM)	4,725	6,625	9,449	14,454	25,400
Pu-239 (g/MTIHM)	81,611	92,350	105,390	135,150	160,200
Pu-240 (g/MTIHM)	34,379	46,323	64,240	97,610	160,530
Pu-241 (g/MTIHM)	6,554	8,458	11,967	19,677	30,919
Am-241 (g/MTIHM)	6,408	8,017	11,022	17,343	26,575
Sr-90 (g/MTIHM)	510	676	869	1,079	1,763
Y-90 (g/MTIHM)	0.13	0.17	0.22	0.27	0.44
Cs-137 (g/MTIHM)	2,370	3,252	4,306	5,529	9,457
Ba-137 (g/MTIHM)	425	601	790	964	1,737
U-235/U	0.11%	0.10%	0.10%	0.10%	0.13%
TRU/HM	16.4%	20.7%	27.4%	41.1%	71.5%

Table 4.18 Charge Data for the Startup Fuel Cycle for Oxide-Fueled ABR

Reference CR	1.00	0.75	0.50	0.25	0.00
Actual Conversion Ratio	0.97	0.76	0.54	0.32	0.11
Heavy Metal (g/MTIHM)	1,000,000	1,000,000	1,000,100	1,000,000	1,000,000
Plutonium (g/MTIHM)	158,290	211,580	297,760	445,800	700,600
Neptunium (g/MTIHM)	8,328	11,129	15,660	23,448	36,858
Americium (g/MTIHM)	8,599	11,490	16,165	24,206	38,041
Curium (g/MTIHM)	1,017	1,359	1,912	2,863	4,498
U-235 (g/MTIHM)	1,631	1,515	1,328	1,006	452
Pu-238 (g/MTIHM)	4,044	5,406	7,606	11,391	17,900
Pu-239 (g/MTIHM)	84,168	112,520	158,320	237,110	372,580
Pu-240 (g/MTIHM)	39,736	53,100	74,710	111,890	175,800
Pu-241 (g/MTIHM)	18,748	25,056	35,258	52,790	82,990
Am-241 (g/MTIHM)	5,951	7,950	11,185	16,752	26,323
U-235/U	0.20%	0.20%	0.20%	0.20%	0.21%
TRU/HM	17.6%	23.6%	33.1%	49.6%	78.0%
BOEC HM (kg)	19,277	15,244	10,900	6,852	3,903
BOEC TRU (kg)	3,606	3,637	3,531	3,246	2,959
Reprocessed TRU Feed Rate[1] (kg/year)	0	0	0	0	0
Makeup TRU Feed Rate[1] (kg/year)	515	540	600	650	798
HM Charge Rate[1] (kg/year)	2,922	2,294	1,809	1,310	1,023

[1]Assumes 85% capacity factor

Table 4.19 Five-Year Cooled Data for the Startup Fuel Cycle for Oxide-Fueled ABR

Reference Conversion Ratio	1.00	0.75	0.50	0.25	0.00
Average Discharge Burnup, GWd/MTIHM	102.7	130.9	166.0	229.2	293.9
Heavy Metal (g/MTIHM)	890,700	861,100	823,400	752,600	684,400
Plutonium (g/MTIHM)	161,290	186,910	228,450	294,800	434,740
Neptunium (g/MTIHM)	3,956	4,906	6,440	8,742	15,393
Americium (g/MTIHM)	10,326	13,310	18,053	25,606	40,383
Curium (g/MTIHM)	1,627	2,247	3,299	5,267	7,823
Fission Products (g/MTIHM)	102,640	129,200	162,660	225,180	284,460
U-235 (g/MTIHM)	619	546	477	369	264
Pu-238 (g/MTIHM)	6,226	8,158	11,405	16,821	26,244
Pu-239 (g/MTIHM)	92,830	98,850	108,310	120,940	163,420
Pu-240 (g/MTIHM)	44,033	55,920	75,130	107,050	164,500
Pu-241 (g/MTIHM)	6,941	9,048	12,635	18,706	31,119
Am-241 (g/MTIHM)	7,056	8,973	11,955	16,502	26,389
Sr-90 (g/MTIHM)	691	850	1,044	1,407	1,757
Y-90 (g/MTIHM)	0.17	0.21	0.26	0.35	0.44
Cs-137 (g/MTIHM)	3,295	4,156	5,267	7,360	9,439
Ba-137 (g/MTIHM)	713	910	1,130	1,537	1,782
U-235/U	0.09%	0.08%	0.08%	0.09%	0.14%
TRU/HM	19.9%	24.1%	31.1%	44.4%	72.8%

4.7. Reference ABR Safety Parameters

This study quantified a large set of reactivity coefficients and kinetics parameters, so the general trends can be quantified. Based solely on static parameters, a safety assessment cannot be made because it is the interaction of these parameters that determines the reactor response to different scenarios. A change in magnitude of many of the parameters would be beneficial for some scenarios and detrimental for others. Detailed safety analysis is required to determine if sufficient safety margins exist. This analysis has not been performed for these designs. The safety performance of these reactors, particularly at very low conversion ratios, may limit the designs and impose additional design constraints. However, a detailed safety analysis performed for a CR=0.25 metal-fueled 840 MWt design [17] suggested that low conversion ratio sodium-cooled fast reactors would be safe (at least with metal fuel).

Table 4.20 and Table 4.21 provide the kinetics parameters and reactivity coefficients estimated for the BOEC and EOEC configurations of the ABR metal and oxide-fueled cores. Many parameters trend in a less than desirable direction, but increased feedback from thermal expansion of the core and increased prompt neutron lifetime may be adequate to compensate. The relative direction of the trends in these parameters is discussed briefly in this section.

Table 4.20 Kinetics Parameters and Reactivity Coefficients of Metal-Fueled ABR Cores

		ABTR	Blanket-free	Compact Core				
Conversion Ratio		0.65	1.00	1.00	0.75	0.50	0.25	0.00
Effective delayed neutron fraction	BOEC	0.0033	0.0035	0.0035	0.0033	0.0030	0.0027	0.0024
	EOEC	0.0033	0.0034	0.0035	0.0033	0.0030	0.0027	0.0024
Prompt neutron lifetime, μs	BOEC	0.33	0.33	0.29	0.32	0.37	0.44	0.52
	EOEC	0.33	0.33	0.29	0.32	0.38	0.45	0.53
Radial expansion coefficient, ¢/ºC	BOEC	-0.59	-0.29	-0.28	-0.35	-0.41	-0.48	-0.57
	EOEC	-0.60	-0.29	-0.29	-0.35	-0.43	-0.50	-0.60
Axial expansion coefficient, ¢/ºC	BOEC	-0.06	-0.29	-0.30	-0.42	-0.52	-0.63	-0.75
	EOEC	-0.05	-0.30	-0.31	-0.44	-0.54	-0.67	-0.80
Fuel density coefficient, ¢/ºC	BOEC	-0.75	-0.59	-0.58	-0.69	-0.80	-0.93	-1.10
	EOEC	-0.76	-0.61	-0.60	-0.71	-0.84	-0.99	-1.18
Structure density coefficient, ¢/ºC	BOEC	0.03	0.09	0.08	0.08	0.09	0.10	0.11
	EOEC	0.03	0.09	0.08	0.08	0.09	0.11	0.12
Sodium void worth, $	BOEC	1.75	8.40	6.29	6.82	9.17	10.18	10.82
	EOEC	1.85	8.76	6.46	7.12	9.78	10.99	11.87
Sodium density coefficient, ¢/ºC	BOEC	0.03	0.18	0.13	0.15	0.18	0.18	0.19
	EOEC	0.03	0.19	0.14	0.15	0.19	0.20	0.21
Doppler coefficient, ¢/ºC	BOEC	-0.10	-0.12	-0.11	-0.10	-0.08	-0.06	-0.01
	EOEC	-0.10	-0.12	-0.10	-0.10	-0.09	-0.06	-0.01
Voided Doppler coefficient, ¢/ºC	BOEC	-0.07	-0.08	-0.07	-0.07	-0.05	-0.03	-0.01
	EOEC	-0.07	-0.07	-0.07	-0.07	-0.05	-0.03	-0.01
Reactivity swing, Δk		1.18%	0.10%	-0.06%	1.47%	2.90%	3.56%	4.17%
Transient initiator ($/rod)		0.51	0.03	0.02	0.28	0.60	0.59	0.78
Reactivity swing ($/EFPY)		N/A	0.18	0.16	7.04	15.91	30.15	47.38

Table 4.21 Kinetics Parameters and Reactivity Coefficients of Oxide-Fueled ABR Cores

		ABTR	Blanket-free	Compact Core				
Conversion Ratio		0.64	1.00	1.00	0.75	0.50	0.25	0.00
Effective delayed neutron fraction	BOEC	0.0032	0.0035	0.0035	0.0033	0.0030	0.0027	0.0024
	EOEC	0.0032	0.0034	0.0035	0.0033	0.0030	0.0027	0.0024
Prompt neutron lifetime, μs	BOEC	0.42	0.33	0.29	0.32	0.37	0.44	0.52
	EOEC	0.42	0.33	0.29	0.32	0.38	0.45	0.53
Radial expansion coefficient, ¢/ºC	BOEC	-0.55	-0.29	-0.28	-0.35	-0.41	-0.48	-0.57
	EOEC	-0.56	-0.29	-0.29	-0.35	-0.43	-0.50	-0.60
Axial expansion coefficient, ¢/ºC	BOEC	-0.06	-0.29	-0.30	-0.42	-0.52	-0.63	-0.75
	EOEC	-0.06	-0.30	-0.31	-0.44	-0.54	-0.67	-0.80
Fuel density coefficient, ¢/ºC	BOEC	-0.51	-0.59	-0.58	-0.69	-0.80	-0.93	-1.10
	EOEC	-0.58	-0.61	-0.60	-0.71	-0.84	-0.99	-1.18
Structure density coefficient, ¢/ºC	BOEC	0.03	0.09	0.08	0.08	0.09	0.10	0.11
	EOEC	0.04	0.09	0.08	0.08	0.09	0.11	0.12
Sodium void worth, $	BOEC	1.32	8.40	6.29	6.82	9.17	10.18	10.82
	EOEC	1.40	8.76	6.46	7.12	9.78	10.99	11.87
Sodium density coefficient, ¢/ºC	BOEC	0.01	0.18	0.13	0.15	0.18	0.18	0.19
	EOEC	0.01	0.19	0.14	0.15	0.19	0.20	0.21
Doppler coefficient, ¢/ºC	BOEC	-0.20	-0.12	-0.11	-0.10	-0.08	-0.06	-0.01
	EOEC	-0.20	-0.12	-0.10	-0.10	-0.09	-0.06	-0.01
Voided Doppler coefficient, ¢/ºC	BOEC	-0.16	-0.08	-0.07	-0.07	-0.05	-0.03	-0.01
	EOEC	-0.16	-0.07	-0.07	-0.07	-0.05	-0.03	-0.01
Reactivity swing, Δk		1.35%	0.10%	-0.06%	1.47%	2.90%	3.56%	4.17%
Transient initiator ($/rod)		0.60	0.03	0.02	0.28	0.60	0.59	0.78
Reactivity swing ($/EFPY)		N/A	0.18	0.16	7.04	15.91	30.15	47.38

4.7.1. Transient Overpower Initiator

The burnup reactivity swing was estimated by the excess reactivity that must be controlled, but a detailed control rod worth calculation was not performed. The results are for the average control assembly, while the most reactive assembly will be limiting. Figure 4.14 shows the burnup reactivity swing in terms of reactivity in dollars per full power year of operation. The value was calculated by dividing the reactivity swing of an individual cycle by the cycle length. The transient initiator value as estimated by initial excess reactivity per primary control assembly is proportional to the cycle length and inversely proportional to the number of primary control assemblies. For example, the CR=0.0 metal-fueled core has a reactivity swing of nearly $45 per full power year (FPY). Therefore, if the average reactivity per primary control assembly is limited to $0.5, a cycle length of 0.5 FPY would require 45 primary control assemblies.

There is a tradeoff between shorter cycle lengths, more control assemblies, and higher maximum control assembly reactivity at power. These tradeoffs can only be understood with detailed safety and economics analysis. Design modifications might be necessary to accommodate the much large number of control rods necessary for very low conversion ratios. Greater numbers of control rods could impact the design of the vessel heads and design of the refueling equipment. All of this is beyond the scope of this analysis.

The results show that it will be far simpler to accommodate the burnup reactivity swing at higher conversion ratios than at very low conversion ratios. The higher specific power for the metal-fueled core results in slightly higher reactivity swing rate than for the oxide core at a given conversion ratio, except at very high conversion ratios where the burnup reactivity swing is essentially zero. All burnup reactivity swings shift to higher values for the startup core, which make this even slightly more problematic.

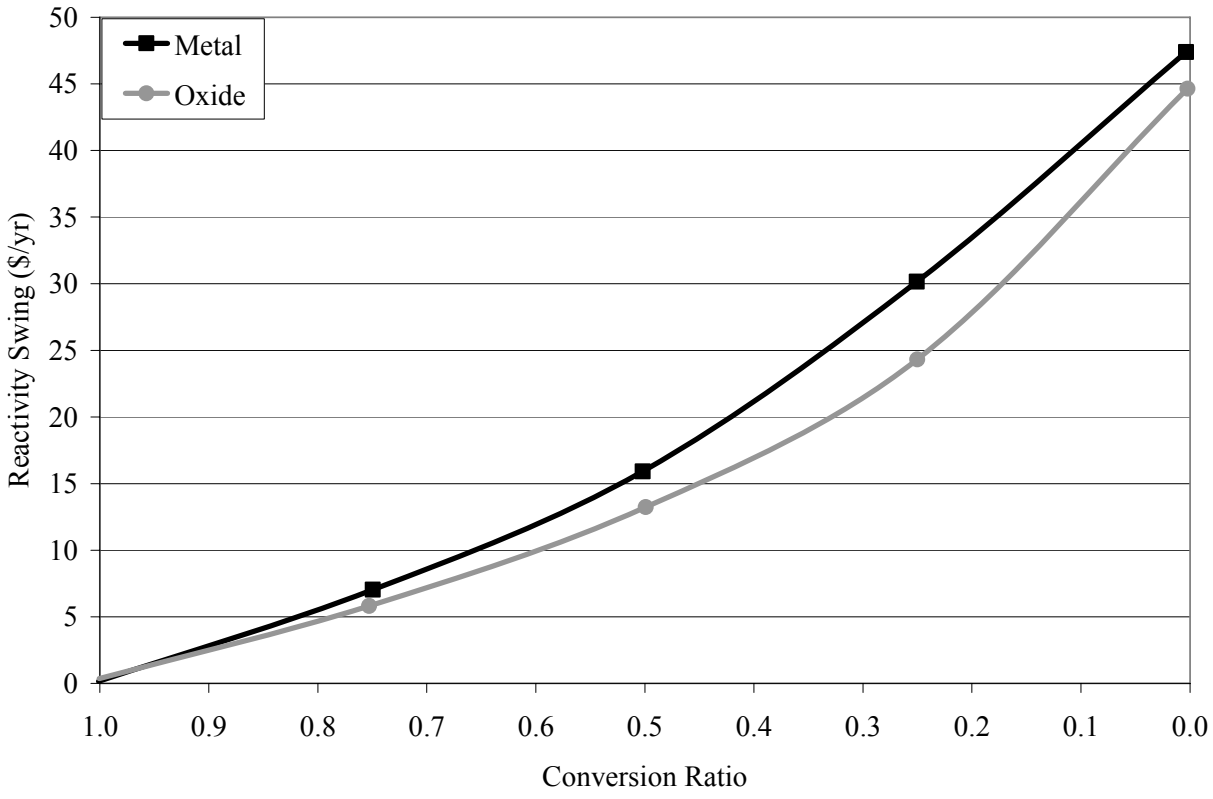

Figure 4.14 Burnup Reactivity Swing Dependence on Conversion Ratio

4.7.2. Sodium Void Worth

Figure 4.15 shows the sodium void worth. As the conversion ratio is reduced, the fuel has an increased TRU inventory and a larger coolant volume fraction. The increased TRU inventory and coolant volume fraction are the primary factors that lead to increased coolant void worth at lower conversion ratios. The void worth of the metal-fueled core is larger than the oxide-fueled core at high conversion ratios, but it is significantly lower at very low conversion ratios because of the lower TRU inventory and coolant volume fraction. For the CR=0.0 designs, the TRU inventory is 3.57 MT for the metal-fueled core and 3.88 MT for the oxide-fueled core and the coolant volume fraction is 44% for the metal-fueled core and 65% for the oxide-fueled core. At a conversion ratio of 0.25, the metal-fueled reactor would have nearly double the void worth of the breakeven core, but would have approximately 40% lower void worth than the oxide-fueled core. The need for gas expansion modules (GEMs) and their reactivity effect was not evaluated.

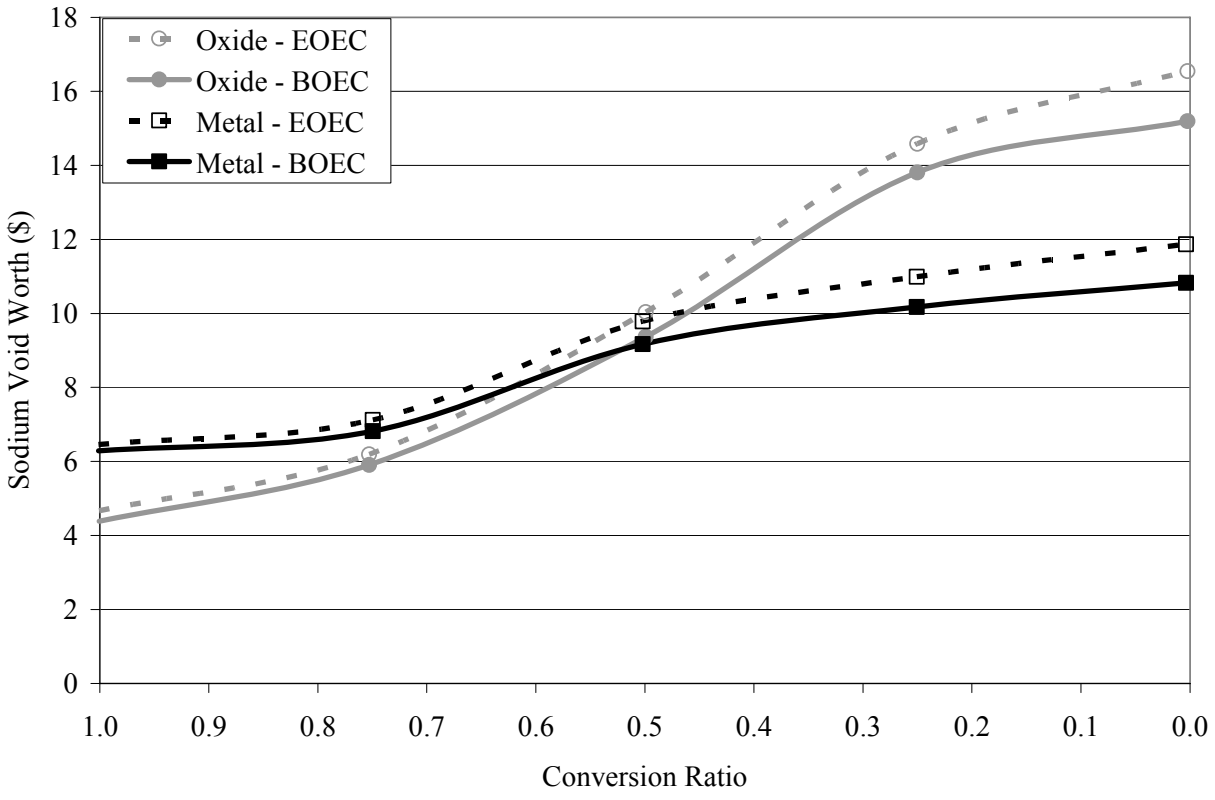

Figure 4.15 Sodium Void Worth Dependence on Conversion Ratio

4.7.3. Expansion Coefficients

Figure 4.16 shows the radial and axial expansion coefficients for metal and oxide-fueled cores at the end of cycle. The low conversion ratio cores show far more negative expansion coefficients than the higher conversion ratios. The metal values are more negative than the oxide values. Thermal expansion is another safety coefficient that trends in the generally more favorable direction and would provide the negative feedback necessary to offset positive reactive insertions from different accident scenarios. However, larger magnitude expansion coefficients increase the reactivity at cold conditions relative to hot conditions, which require more control assembly worth to have sufficient shutdown margin.

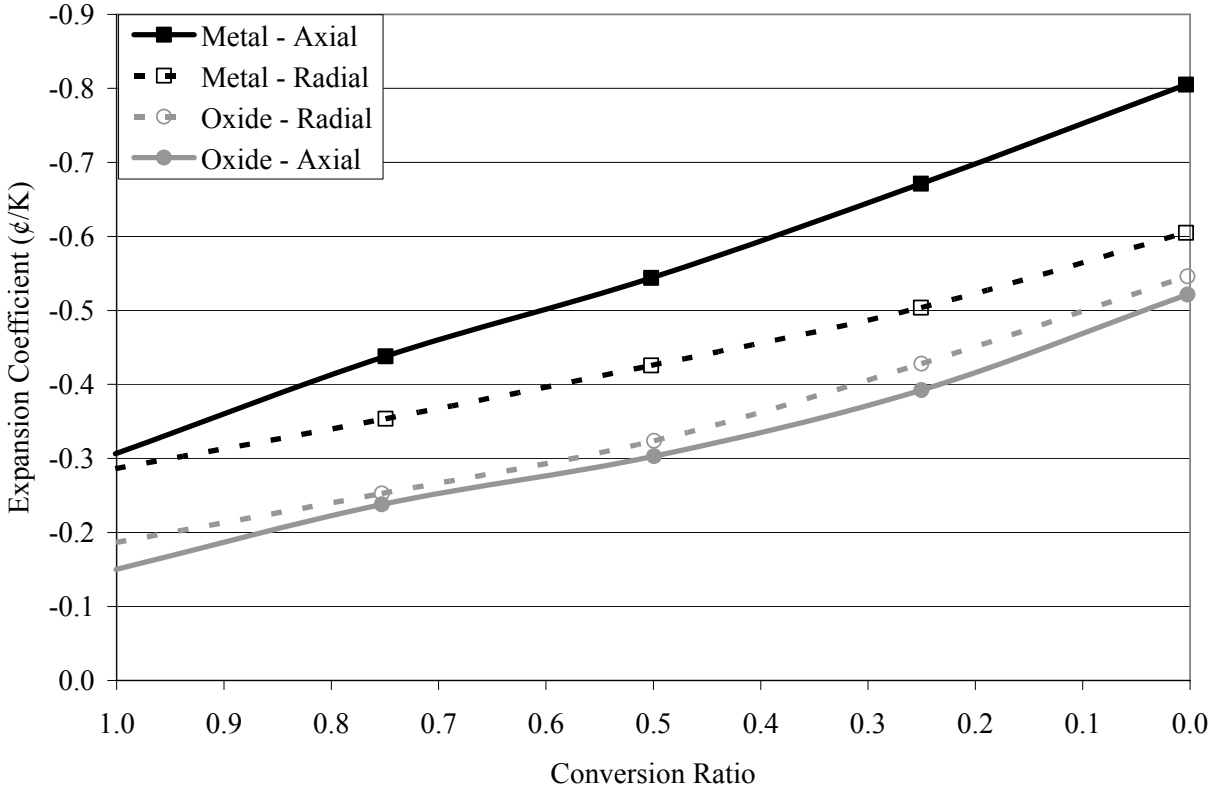

Figure 4.16 Expansion Coefficient Dependence on Conversion Ratio

4.7.4. Doppler Fuel Temperature Coefficient

Figure 4.17 shows the Doppler fuel temperature coefficients for metal and oxide-fueled cores. The Doppler fuel temperature coefficient becomes increasingly less negative at lower conversion ratios. This is a result of the greatly reduced concentration of U-238 at high conversion ratios. The Doppler fuel temperature coefficient is significantly more negative for the oxide fuel than the metal fuel at high conversion ratios, but the difference is greatly reduced at very low conversion ratios.

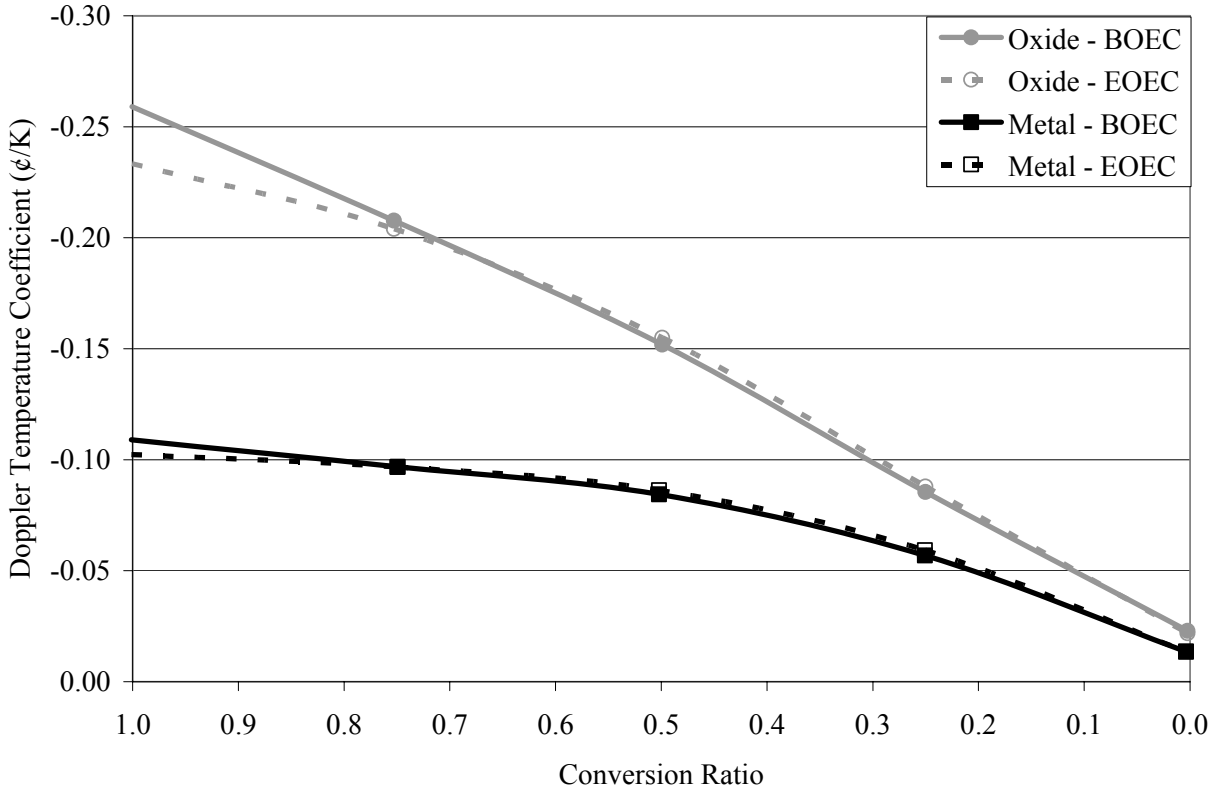

Figure 4.17 Doppler Fuel Temperature Coefficient Dependence on Conversion Ratio

4.7.5. Prompt Neutron Lifetime

Figure 4.18 shows the prompt neutron lifetime as a function of conversion ratio. The prompt neutron lifetime shows a large increase because of the greatly reduced fuel volume fraction. The prompt neutron lifetime nearly doubles from conversion ratio of 1.0 to zero. The prompt neutron lifetime of the oxide core is significantly longer than the metal-fueled core. This will likely have very significant impact on the time behavior of any transient and reactor response.

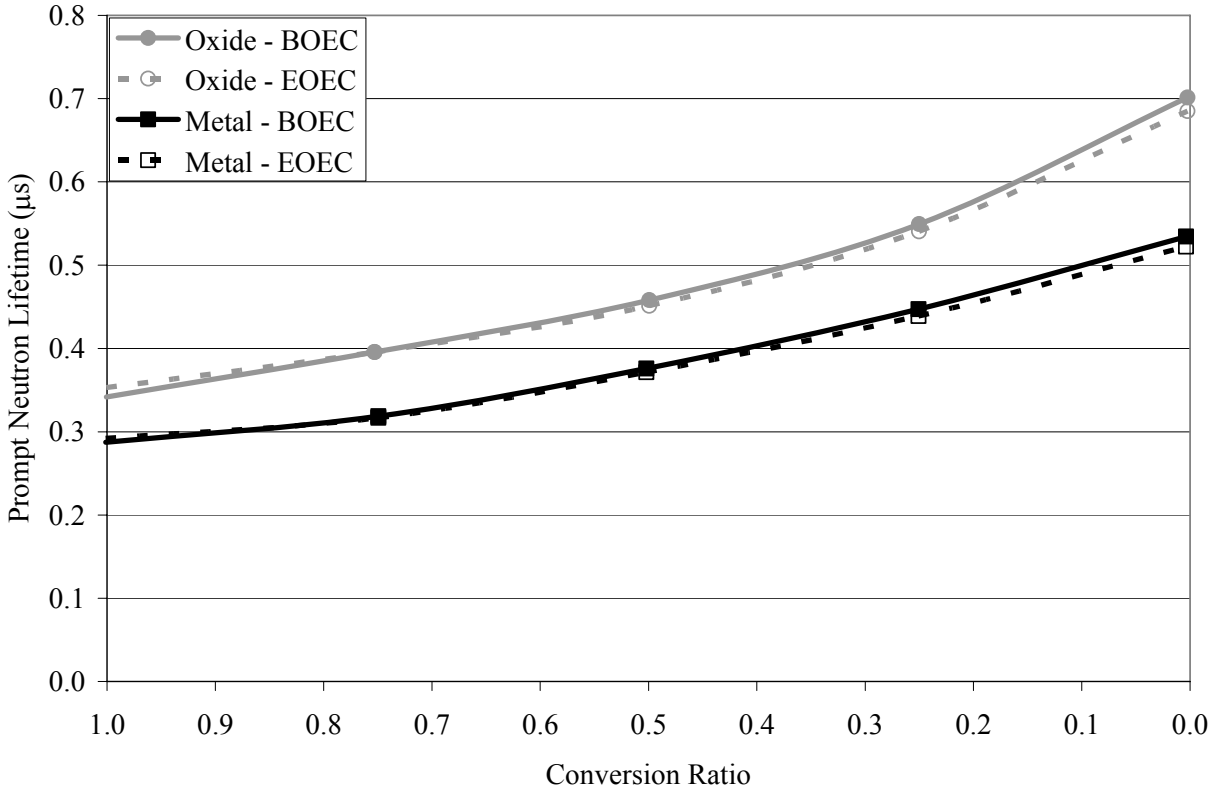

Figure 4.18 Prompt Neutron Lifetime Dependence on Conversion Ratio

4.7.6. Delayed Neutron Fraction

Figure 4.19 shows the delayed neutron fraction for metal and oxide-fueled cores. The delayed neutron fraction decrease significantly at lower conversion ratios. The reduced contribution of the fast fission of U-238 is the primary reason for the declining value. The metal fuel is somewhat higher at high conversion ratios, but the difference is negligible at very low conversion ratios. The reduced delayed neutron fraction will increase the prompt response to reactivity insertions.

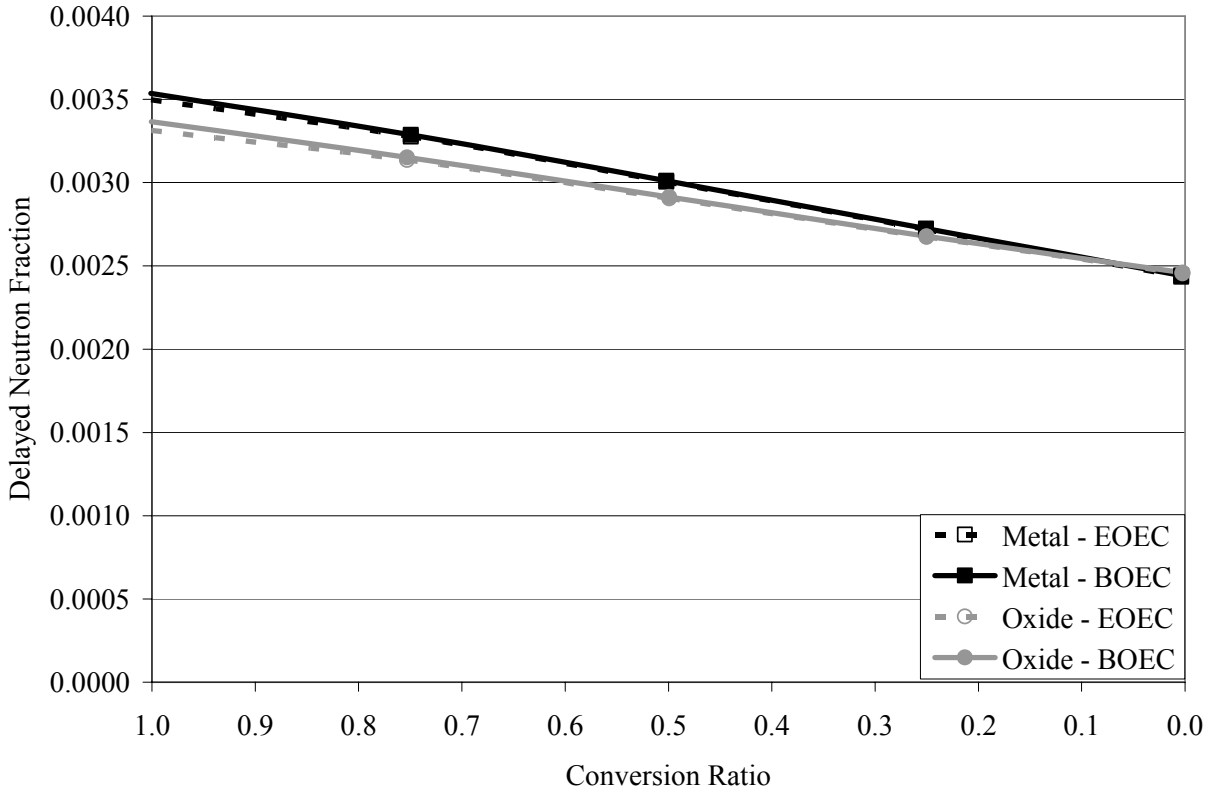

Figure 4.19 Delayed Neutron Fraction Dependence on Conversion Ratio

5.0 Conclusion

Core design studies have been performed to develop ABR designs for both metal and oxide-fueled cores with conversion ratios from breakeven (CR=1.0) to fertile-free (CR=0.0). The designs were developed for a commercial-scale sodium-cooled fast reactor. The designs are based on the S-PRISM design which is a modular power plant based on 1000 MWt reactor cores. The ABR core designs were developed by modifying the S-PRISM core and assembly design to produce the desired conversion ratio in a more compact core, while satisfying thermal and irradiation damage limits. Safety and kinetic parameters were calculated, but a safety analysis was not performed.

The S-PRISM was designed to be a slight to moderate breeding reactor, which contains breeding blankets. For consistency with the lower conversion ratio designs, the first modification was to remove blankets and develop a breakeven design which would fit in the S-PRISM core layout. This layout is unnecessarily large because of the blankets in the S-PRISM design. The number of fuel assemblies (driver and blanket) was reduced by over 35% for the metal-fueled designs and by nearly 50% for the oxide-fueled designs. There are slight variations with conversion ratio but the basic ABR configuration consists of 144 fuel assemblies and between 9 and 22 primary control assemblies for both the metal and oxide-fueled cores. Preliminary design studies indicated that it is feasible to design the ABR to accommodate a wide range of conversion ratio by employing different assembly designs and including sufficient control assemblies to accommodate the large reactivity swing at low conversion ratios.

Current irradiation experience would allow for a conversion ratio of somewhat below 0.75. The fuel qualification for the first ABR should expand this experience to allow for much lower conversion ratios. The current designs were based on assumptions about the performance of high and very high enrichment fuel, which results in significant uncertainty about the details of the designs. However, the basic parameters such as conversion ratio and mass flow parameters are less sensitive to these parameters and the current results should provide a good basis for static and dynamic system analysis. As better fuel performance data is gathered, the designs can be updated.

The conversion ratio is fundamentally a ratio of the U-238 capture cross section to the TRU fission cross sections. Since these cross sections only change moderately with fuel design and isotopic concentration for the fast reactor, a specific conversion ratio requires a specific enrichment. The approximate average charge enrichment (TRU/HM) is 14%, 21%, 33%, 56%, and 100% for conversion ratios of 1.0, 0.75, 0.50, 0.25, and 0.0 for the metal-fueled core. The approximate average charge enrichment is 17%, 25%, 38%, 60%, and 100% for conversion ratios of 1.0, 0.75, 0.50, 0.25, and 0.0 for the oxide-fueled core. For the split batch cores, the maximum enrichment will be somewhat higher.

For both the metal and oxide-fueled cores, the reactivity feedback coefficients and kinetics parameters seem reasonable. The maximum single control assembly reactivity faults may be too

large for the low conversion ratio designs. The average reactivity of the primary control assemblies was increased, which may cause the maximum reactivity of the central control assembly to be excessive. The values of the reactivity coefficients and kinetics parameters show that some values appear to improve significantly at lower conversion ratios while others appear far less favorable. Detailed safety analysis is required to determine if these designs have adequate safety margins or if appropriate design modifications are required.

Detailed system analysis data has been generated for both metal and oxide-fueled core designs over the entire conversion ratio range of potential burner reactors. Additional data has been calculated for a few alternative fuel cycles. The systems data has been summarized in this report and the detailed data will be provided to the systems analysis teams so that static and dynamic system analyses can be performed.

References

1. A.E. Dubberley, K. Yoshida, C.E. Boarman, and T. Wu, "SuperPRISM Oxide and Metal Fuel Core Designs," Proceedings of ICONE 8, 8th International Conference on Nuclear Engineering (2000).
2. C. E. Lahm, J. F. Koenig, R. G. Pahl, D. L. Porter, and D. C. Crawford, "Experience with Advanced Driver Fuels in EBR-II," *Journal of Nuclear Materials*, **204**, 119 (1993).
3. R. B. Baker, F. E. Bard, R. D. Leggett, and A. L. Pinter, "Status of Fuel, Blanket, and Absorber Testing in the Fast Flux Test Facility," *Journal of Nuclear Materials*, **204**, 109 (1993).
4. A. L. Pinter and R. B. Baker, "Metal Fuel Test Program in the FFTF," *Journal of Nuclear Materials*, **204**, 124 (1993).
5. K. L. Derstine, "DIF3D: A Code to Solve One-, Two-, and Three-Dimensional Finite Difference Diffusion Theory Problems," ANL-82-64, Argonne National Laboratory (1984).
6. B. J. Toppel, "A User's Guide to the REBUS-3 Fuel Cycle Analysis Capability," ANL-83-2, Argonne National Laboratory (1983).
7. "NSEC No. 350 ETOE-2 Documentation," National Energy Software Center Note 83-84, August 25, 1983.
8. H. Henryson II, B. J. Toppel, and C. G. Stenberg, "MC^2-2: A Code to Calculate Fast Neutron Spectra and Multi-group Cross Sections," ANL-8144, Argonne National Laboratory (1976).
9. W. M. Stacey, Jr., et al, "A New Space-Dependent Fast Neutron Multigroup Cross Section Preparation Capability," *Trans. Am. Nucl. Soc*., 15, 292 (1972).
10. R. D. Lawrence, "The DIF3D Nodal Neutronics Option for Two- and Three-Dimensional Diffusion Theory Calculations in Hexagonal Geometry," ANL-83-1, Argonne National Laboratory (1983).
11. C. H. Adams, "Specifications for VARI3D – A Multidimensional Reactor Design Sensitivity Code," FRA-TM-74, Argonne National Laboratory (1975).
12. T. A. Daly and B. R. Chandler, "ORIGEN-RA – A Modified Version of the ORIGEN Code," F6500-0019-AQ, Argonne National Laboratory (1994).
13. G. Hofman, L. Leibowitz, J. M. Kramer, M.C. Billone, and J. F. Koenig, Private Communication, Argonne National Laboratory, November 1985.
14. A. D. Pelton and L. Leibowitz, Private Communication, Argonne National Laboratory, August 1988.
15. J. J. Carbajo, G. L. Yoder, S. G. Popov, and V. K. Ivanov, "A Review of the Thermo-physical Properties of MOX," *Journal of Nuclear Materials*, **299**, 181 (2001).
16. R. N. Hill, Private Communication, Argonne National Laboratory, March 2006.
17. J. E. Cahalan and F. E. Dunn, Private Communication, Argonne National Laboratory.
18. T. K. Kim, Private Communication, Argonne National Laboratory.

19. Fast Reactor Database, International Atomic Energy Agency, IAEA-TECDOC-866, 1996.

Nuclear Engineering Division
Argonne National Laboratory
9700 South Cass Avenue, Bldg. 208
Argonne, IL 60439-4842

www.anl.gov

A U.S. Department of Energy laboratory managed by UChicago Argonne, LLC